9-8-2016

Simulation and Analysis of Gradient Frequency Neural Networks

AmirAli Farokhniaee
University of Connecticut, aafarokh@gmail.com

Simulation and Analysis of Gradient Frequency Neural Networks

AmirAli Farokhniaee, PhD

Univeristy of Connecticut, 2016

The methodologies introduced and applied in this work have fundamental roles in connecting the component level descriptions of brain dynamics (single neurons) to population level (neural networks).

The synchronization regions of a single neuron with respect to a periodic external stimulus either deterministic or noisy is evaluated. Many neurons in the auditory system of the brain must encode periodic signals. These neurons under periodic stimulation display rich dynamical states including mode-locking and chaotic responses. Periodic stimuli such as sinusoidal waves and amplitude modulated (AM) sounds can lead to various forms of $n : m$ mode-locked states, in which a neuron fires n action potentials per m cycles of the stimulus. The regions of existence of various mode-locked states on the frequency-amplitude plane, called Arnold tongues, are obtained numerically for Izhikevich neurons. Arnold tongues analysis provides useful insight into the organization of mode-locking behavior of neurons under periodic forcing. We found these tongues for both class-1 (integrator) and class-2 (resonator) neurons, with and without noise. These results are applied in real data and Arnold tongues of a real neuron are obtained using methods of circular statistics such as vector strength. Rayleigh statistical test and Monte Carlo method are necessary to detect and confirm phase-locking (in general mode-locking) in noisy data. These are done for a well-isolated inferior colliculus rabbit cell using acoustic stimuli in the rabbit's ear canal and 2:1 mode-locked behavior of the cell is confirmed.

AmirAli Farokhniaee - Univesity of connecticut, 2016

Next a canonical model for Wilson-Cowan oscillators is derived by doing step by step mathematical analysis. Among these steps we applied some mathematical theorems in stability analysis and dynamical systems. We took advantage of normal form theory after Henri Poincaré, to obtain a canonical model of a neural oscillator model for single and coupled populations. This canonical model exhibits all kinds of bifurcations. As an important case in theoretical neuroscience, we showed how we can simplify the model to obtain Hopf bifurcation. We obtained the governing equations of each oscillator under this bifurcation, which gave us the dynamical behavior and time evolution of each oscillator's amplitude and phase. A novel and straightforward way is presented to solve the average relative phase of two coupled oscillators based on wave solutions applied in wave mechanics via mathematical physics. This approach gives us a complete analytic method to solve for the average relative phase equations of two coupled neurons or neural populations without applying averaging theory, which is lengthy and complicated. These solutions are important in physical sciences, including complex dynamical systems such as theoretical and computational neuroscience.

Simulation and Analysis of Gradient Frequency Neural Networks

AmirAli Farokhniaee

B.Sc., University of Tehran, 2009

M.Sc., Florida Atlantic University, 2012

A Dissertation

Submitted in Partial Fulfillment of the

Requirements for the Degree of

Doctor of Philosophy

at the

University of Connecticut

2016

APPROVAL PAGE

Doctor of Philosophy Dissertation

Simulation and Analysis of Gradient Frequency Neural Networks

presented by

AmirAli Farokhniaee, B.Sc., M.Sc.

Major Adviser _____

Edward Large

Associate Adviser _____

Susanne Yelin

Associate Adviser _____

George Gibson

Associate Adviser _____

Sabato Santaniello

University of Connecticut

2016

Acknowledgements

Foremost, I am thankful to all my committee members for their steadfast integrity and selfless dedication to my personal and academic development.

- Thank you to Dr. Edward Large, for his patience, encouragement and all his supports throughout my Ph.D.

- Thank you to Dr. Susanne Yelin, for her supports and being a great example of professional dedication

- Thank you to Dr. George Gibson, for his helps and enlightening discussions

- Thank you to Dr. Sabato Santaniello, for his patience, great support, dedication and opening new insights into my future.

- Thank you to Dr. Gerald Dunn, for his kind, helpful consultations and immense knowledge were key motivations throughout my Ph.D. .

Special thanks to my mom and dad, and my sister and brother, without them non of these would be possible. To my mom who devoted all her life to raise her children in the best and happiest possible way. To my dad that his efforts and advice have been lighting up my life. Thank you to my dear Elena, she always inspired me to have a deep and fundamental insight into life and academia and helped me overcome challenges. I would like to thank department of physics and all my friends at UConn for being so supportive and great.

The wise are the fixed point of existance compass, but,

Love knows that they are circling around.

-Hafez Shirazi

Persian poet, 1326-1390 CE

Contents

List of Figures

Chapter 1

Synchronization and Mode-locking

1.1 Introduction

Mode-locking is a ubiquitous phenomenon in the auditory system. Recent research has uncovered evidence of mode-locking in single-unit extracellular chopper and onset cells of guinea pigs[2, 25], in the auditory midbrain of the fish Pollimyrus in response to acoustic signals[24, 21, 23] and in saccular hair bundle cells when exposed to periodic mechanical deflections[7]. In order to study the mode-locking behavior of a single neuron one must focus on the periodic external forcing (input) and the resulting neuronal spike pattern (output). In the aforementioned studies sinusoidal stimuli was used, therefore in order to address the phase relations seen in these experiments one can use sinusoidal current injections into the model neuron and then measure mode-locking behavior utilizing an Arnold tongue analysis[16, 27].

A neuron is said to be $n : m$ mode-locked to a periodic stimulus if it fires n action potentials in m cycles of the stimulus, where n and m are positive integers. Phase-locking is defined as $1 : 1$ mode-locking. For two mode-locked oscillators the locking condition is as follows[35, 31]:

$$|\phi_{n,m}| < const., \tag{1.1}$$

where $\phi_{n,m}(t) = n\phi_1(t) - m\phi_2(t)$ and $\phi_{n,m}$ is the generalized phase difference also known as the relative phase. It is clear that in the case when $n = m = 1$ Eq. (2.1) becomes $|\phi_1(t) - \phi_2(t)| < const.$. This behavior is indicative of constant phase shift, or phase-locking, which is generally considered the simplest way to describe synchronization[31].

In order to analyze the synchronization of such an oscillator undergoing external forcing, it is constructive to obtain a global map of synchronization regions.

Synchronization between a neuron's action potentials or spike trains and an external input depends on both the amplitude and frequency of the input. Hence, one can obtain regions on the amplitude-frequency plane that are indicative of mode-locking and synchronization of the two signals i.e. synchronization of the injected periodic signal and the neuronal output. Within these regions, which are commonly referred to as Arnold tongues[31], Eq. (2.1) holds.

In the presence of noise, synchronization still occurs. However, in order to measure the stability of the synchronized states one must introduce a measure. This can be done using vector strength (VS) so that synchronization can be measured both with and without the presence of noise in this model. The VS takes a value of 1 if all spike occur at one precise point and 0 for a uniform distribution of phases across the stimulus cycle. The VS gives a good indication as to whether a phase preference exists in the data both with and without noise [25]. There have been studies to measure the stability of the mode-locked patterns using different neuronal models such as Morris-Lecar [30] and leaky integrate and fire (LIF) neurons [15]. Here we measure the stability of the mode-locked states using Izhikevich model.

Arnold tongue diagrams have been produced for Hodgkin-Huxley models[26, 18] and LIF neurons[25]. This is the first paper which utilizes and reports Arnold tongue diagrams for single Izhikevich neurons. Additionally, Arnold tongues are provided for neurons both with and without the presence of noise. The main advantage for computing Arnold tongues with Izhikevich model is the computational and relatively high speed of processing.

In this paper, first we explain the neuronal model (Izhikevich 2003) that will be utilized. We then present a brief description of Class-1 and Class-2 excitable

neurons and obtain Arnold tongues for both classes of excitability. Then we computed the Arnold tongues for the deterministic case and show examples of mode-locking. The formation of harmonics and sub-harmonics in the frequency response of the neuron were then analyzed for some example points in the mode-locking regions. Next we considered mode-locking in the presence of noise. This was done by computing the vector strength to measure the stability of the corresponding mode-locking regions of the Arnold tongues . This analysis was then continued for the noisy model which more accurately simulates biological conditions. The computational and analytic tools developed here can also be applied to physiological spike trains for any type or class of neuron.

1.2 Model and methodology

Izhikevich model

One of the most significant and influential models in computational neuroscience is the Hodgkin-Huxley model of the squid giant axon[12]. This model captures the generation of action potentials by modelling the inward and outward currents into a neuron through voltage-gated ion channels. In general it consists of four coupled non-linear differential equations and many parameters that depend on the electrophysiology of the neuron under study. These parameters are usually obtained by experiment. Hodgkin-Huxley model is complete but not computationally economical.

The spiking model of Izhikevich is a canonical model based on the Hodgkin-Huxley model, with reduced dimensionality. This simple model consists of two

coupled nonlinear differential equations that give the time evolution of the components of the system in phase space [14]:

$$\dot{v} = 0.04v^2 + 5v + 140 - u + I(t) \quad and \quad \dot{u} = a(bv - u) \tag{1.2}$$

$$if \quad v \geq 30 \text{ mv} \quad then \quad v \longleftarrow c \ , \ u \longleftarrow u + d$$

where v is the membrane potential (in mV), u is the membrane recovery variable which accounts for the activation of K^+ ionic currents and inactivation of Na^+ and I is the injected current to the neuron. u provides negative feedback to v. The coefficients are chosen such that both membrane potential v and t are represented in millivolts and milliseconds, respectively. Different values of the parameters a, b, c, d in the model correspond to known types of neurons[14]. This reduced model is derived based on an approximation of the nullclines of the Hodgkin-Huxley model. The Izhikevich model is simple yet incredibly precise, and has broad applications to almost all types of neurons. It exhibits firing patterns of *all* known types and is efficient in large-scale simulation of cortical networks[14]. In order to be more realistic, so that the model can be applied to biological systems, it is preferable to work with another version of the Izhikevich model which is derived based on current-voltage relations. Hence we represent the equivalent form of system of equations in (1.2):

$$C\dot{v} = k(v - v_r)(v - v_t) - u + I(t) \quad and \quad \dot{u} = a[b(v - v_r) - u] \tag{1.3}$$

$$if \quad v \geq v_{peak} \quad then \quad v \longleftarrow c \ , \ u \longleftarrow u + d$$

where C is the membrane capacitance (in nF), v_r is the resting membrane potential, v_t is the instantaneous threshold potential and v_{peak} is the spike cutoff value. a is the recovery constant, c is the voltage reset value, and d is the parameter that describes the total flow of ionic current during the spike and affects the after-spike behavior[12].

As introduced by Izhikevich[12] the sum of all slow currents that modulate the spike generation mechanism is represented by the phenomenological variable u. Depending on sign of b, u is either an amplifying (for $b \leq 0$) or resonating (for $b \geq 0$) variable that defines the class of excitability.

Different classes of neurons

A simple but useful criterion for classifying neuronal excitability was suggested by Hodgkin [10]. He discovered by stimulating a cell by applying currents of various strength that when the current was weak the cell was quiet, conversely when the current became strong the cell began to fire repeatedly. Thus, he divided neurons into two classes according to the frequency of emerging firing: class-1 neural excitability, in which action potentials can be generated with arbitrarily low frequency that increases in accordance with the applied current, and class-2 neural excitability, where action potentials are generated in a certain frequency band that is relatively insensitive to changes in the strength of the applied current. These two classes are reproduced by changing the parameters of Izhikevich model in Figs. 1a and 1b.

As was described earlier, the sign of b determines the neuron's excitability class i.e. one can covert from an integrating regime to a resonating regime by changing

the sign of b. Class-1 neurons, such as regular spiking cortical pyramidal neurons, are monostable integrators i.e. the resting state disappears through a saddle-node on an invariant circle (SNIC) bifurcation. Conversely, Class-2 neurons, such as inferior colliculus cells in the auditory system of the rabbits[3], are bistable resonators[12] i.e. the resting state loses stability via a subcritical Andronov-Hopf bifurcation. One of the reasons of using this classification is its importance and usefulness to understand the emergence of frequency components of neuronal output (harmonics and sub-harmonics) which are computed in section 1.3.

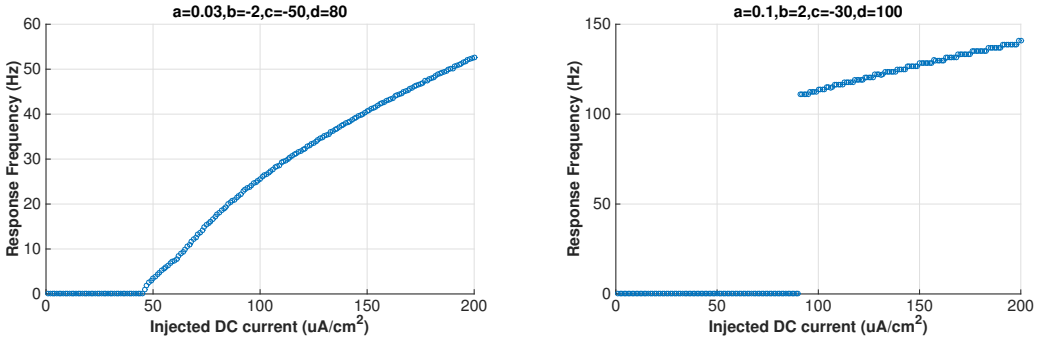

(a) Class-1 F-I curve

(b) Class-2 F-I curve

Figure 1.1: (a) F-I curve for a class-1 neuron plotted for an Izhikevich neuron (Eq. 1.3) with parameters $a = 0.03, b = -2, c = -50, d = 80, C = 100nF, v_r = -64mV, v_t = -40mV, v_{peak} = 35mV$ and $k = 0.7$. (b) F-I curve for a class-2 neuron plotted for an Izhikevich neuron with parameters $a = 0.1, b = 2, c = -30, d = 100, C = 100nF, v_r = -60mV, v_t = -40mV, v_{peak} = 35mV$ and $k = 0.7$.

1.3 Results

To study mode-locking we inject the neuron with an external stimulus that includes a direct current I_{DC} and an alternating current that for our purpose is $I_{AC} = A\sin(\omega t)$ where $\omega = 2\pi f$ with f as the stimulus frequency in Hz. I_{DC} was present to ensure that the neuron was in the firing state. Thus, the value of I_{DC} should be determined by Fig. (1.1) i.e. it should be selected such that the neuron is in the firing state.

1.3.1 Arnold Tongues Diagram for Class-1 Neuron

We computed synchronization families for $n, m \in \{1, 2, 3, 4, 5\}$. Fig. (1.2) shows the regions of amplitude-frequency plane where different mode-locking ratios can be observed. This plot represents the mode-locked regions as a function of the amplitude and frequency of the sinusoidal forcing, with the direct current of $I_{DC} = 62\mu A/cm^2$. As mentioned previously, the n:m ratio is indicative of a mode-locked state. For example, for stimulus amplitudes and frequencies corresponding to the orange region the neuron exhibits $3:1$ mode-locking.

For each element of the amplitude-frequency matrix that forms the plane, we simulated the model for 10 seconds. Then in order to have a stable firing pattern of the neuron, the last 5 seconds of the spiking pattern and corresponding stimulus were considered. If Eq. (2.1) is satisfied, this particular element takes the value of $n:m$, otherwise it takes zero. The same procedure is done to find the other elements of the matrix and form the whole plane in Figs. (1.2) and (1.5). Note that using Eq. (2.1) in a computer code requires defining a tolerance zone, i.e. the constant value defined on the RHS can be any number less than a tolerance zone

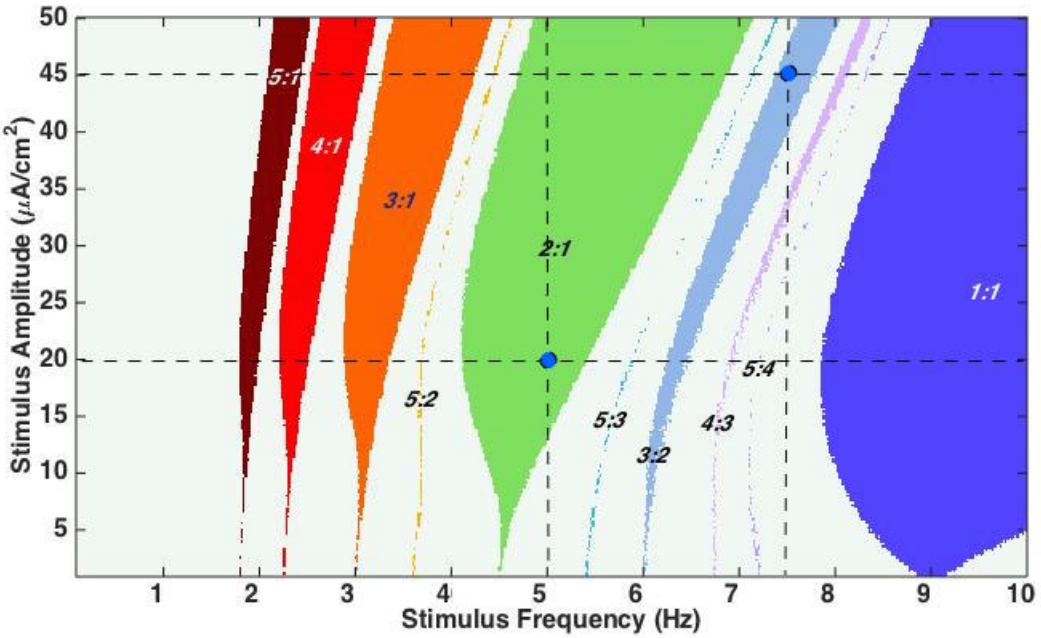

Figure 1.2: Arnold tongues diagram for a class-1 Izhikevich neuron driven by an external sinusoidal forcing that corresponds to the neuron with the F-I curve and parameters shown in Fig. 1.1a. The DC current is 62 ($\mu A/cm^2$).

defined by the user.

We demonstrated the time series of the spiking pattern plus the frequency spectrum of the spike trains for the two different points of this diagram which, as previously mentioned, correspond to two different amplitude and frequencies of the stimulus. For $A = 45\mu A/cm^2$ and $f = 7.5Hz$, we have $3:2$ mode-locking that is presented in Fig.(1.3a). For the corresponding values of A and f, frequency spectrum of the output has been computed by a Fourier transform and presented in Fig.(1.3b) as well. The sharp peak observable in Fig.(1.3b) corresponds to the driving frequency of the neuron, i.e. the frequency of the sinusoidal input ($7.5Hz$). There are peaks that are multiples of this driving frequency, which present the

harmonics of the input. Also, there is a smaller ratio of the driving frequency that corresponds to a sub-harmonic of the input. This example of a $3:2$ mode-locking state has a sub-harmonic frequency of $3.75Hz$ which was calculated by dividing the deriving frequency by 2.(the denominator of the mode-locked state).

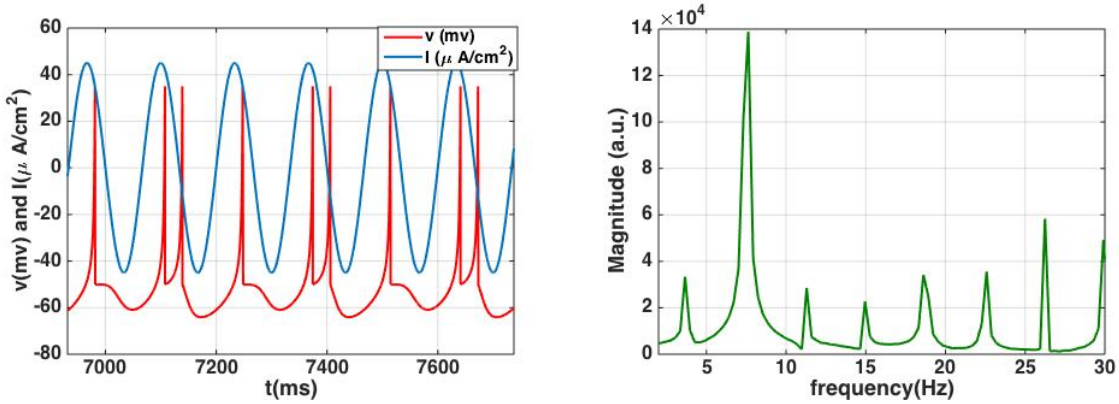

(a) (b)

Figure 1.3: 1^{st} example, $3:2$ mode-locked pattern (a) Time series diagram of a sinusoidal stimulus with amplitude of $A = 45\mu A/cm^2$ and frequency of $f = 7.5Hz$ (blue) and the corresponding spike pattern (red) (b) Frequency spectrum of the spike pattern corresponding to a sinusoidal stimulus with amplitude of $A = 45\mu A/cm^2$ and frequency of $f = 7.5Hz$) .

Another example is $A = 20\mu A/cm^2$ and $f = 5Hz$. The corresponding input-output time series and frequency spectrum of the output can be seen in Fig. (1.4).

The formation of harmonics can be observed in Fig. (1.4b). However, there are no sub-harmonics observed here since the denominator of the mode-locked state is 1.

1.3.2 Arnold Tongues Diagram for Class-2 Neuron

Next, we compute Arnold tongues for a class-2 neuron, Fig. (1.5). In class-2 neurons action potentials are generated in a certain frequency band, which are not

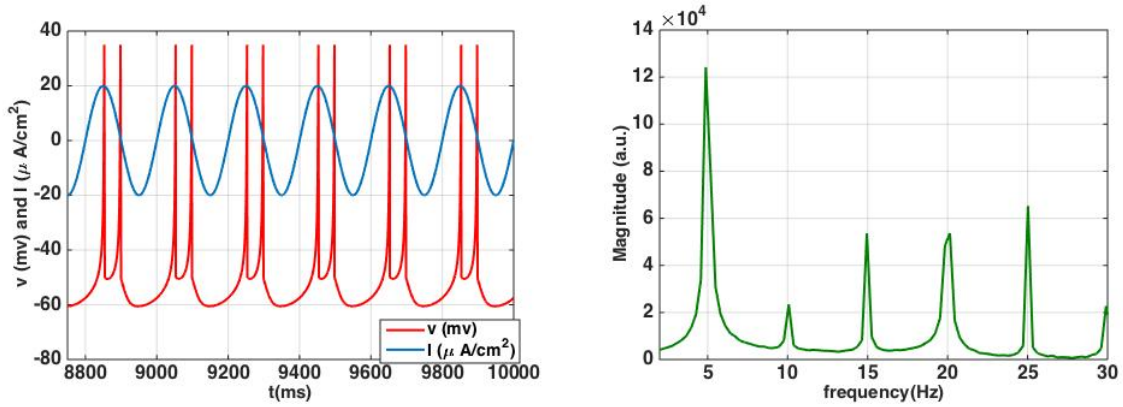

(a) (b)

Figure 1.4: 2^{nd} example, $2:1$ mode-locked pattern (a) Time series diagram of a sinusoidal stimulus with amplitude of $A = 20$ $(\mu A/cm^2)$ and frequency of $f = 5Hz$(blue) and the corresponding spike pattern (red) (b) Frequency spectrum of the spike pattern corresponding to a sinusoidal stimulus with amplitude of $A = 20\mu A/cm^2$ and frequency of $f = 5Hz$.

highly dependent on the applied current (Fig. 1.1b). Hence the tongues in Fig. (1.5) are not tilted as much as the tongues in Fig. 1.2. Furthermore, the tongues occur at relatively higher frequencies (refer to x-axis) than the class-1 neuron. This is consistent with the fast spiking behavior of class-2 neurons, Fig. 1.1b. Again we consider two example points of this diagram in order to visualize the mode-locked behavior. The corresponding time series and frequency spectra are given in Figs. (1.6) and (1.7).

Note the formation of harmonics and sub-harmonics again. The amplitude of sub-harmonics are much greater and more dominant than those seen in class-1 neurons. In Fig. (1.6b) we have the sub-harmonic of the driving frequency 37.5 Hz, which corresponds to 75/2 (driving frequency divided by the denominator of the mode-locked state). In the case of Fig. (1.7b), which depicts the mode-locked region of $2:3$ (smaller than 1), sub-harmonic construction is even more dominant

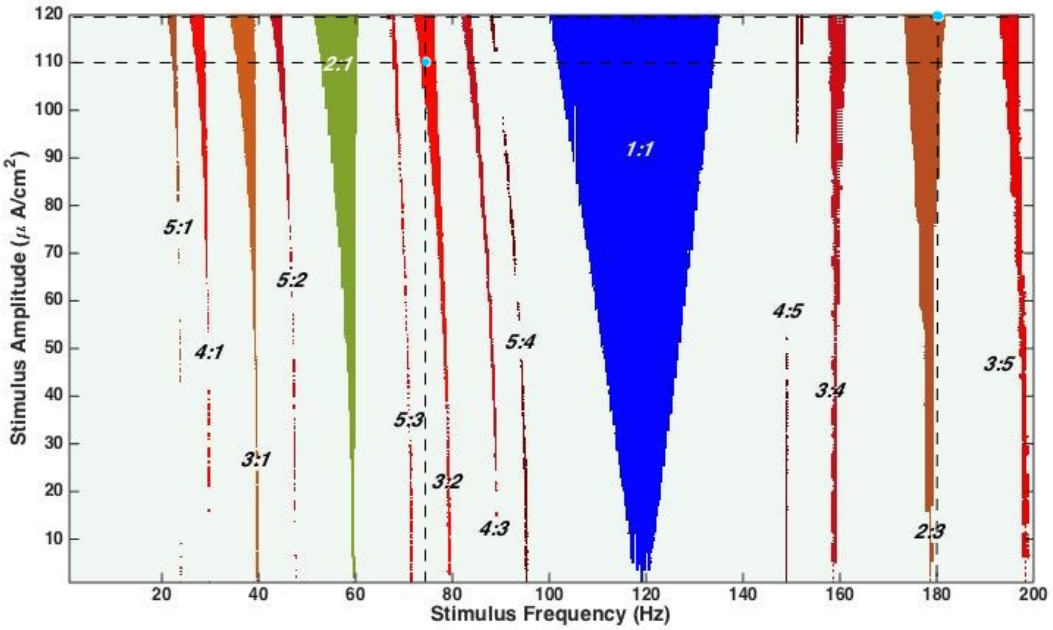

Figure 1.5: Arnold tongues diagram for a class-2 Izhikevich neuron driven by an external sinusoidal forcing that corresponds to the neuron with the F-I curve and parameters shown in Fig. 1.1b. The DC current is ($120\mu A/cm^2$).

than in the case of Fig. (1.6b), additionally it is also greater in amplitude than the subsequent harmonics. In Fig. (1.7b) we have two observed sub-harmonics at 60 and 120 Hz. The first one is the driving frequency divided by 3 ($180/3 = 60\ Hz$) and the second one is $2 \times 60 = 120\ Hz$, since the numerator of the mode-locked state is 2.

As has been previously studied[11, 13, 12] resonators and integrators differ in the way they respond to input. In monostable integrator neurons (Class-1), whose quiescent state disappears through a SNIC bifurcation, the neuron can fire with an arbitrarily low frequency. Conversely, in bistable resonator or integrator neurons (Class-2) the resting potential loses stability via either a saddle-node, subcritical

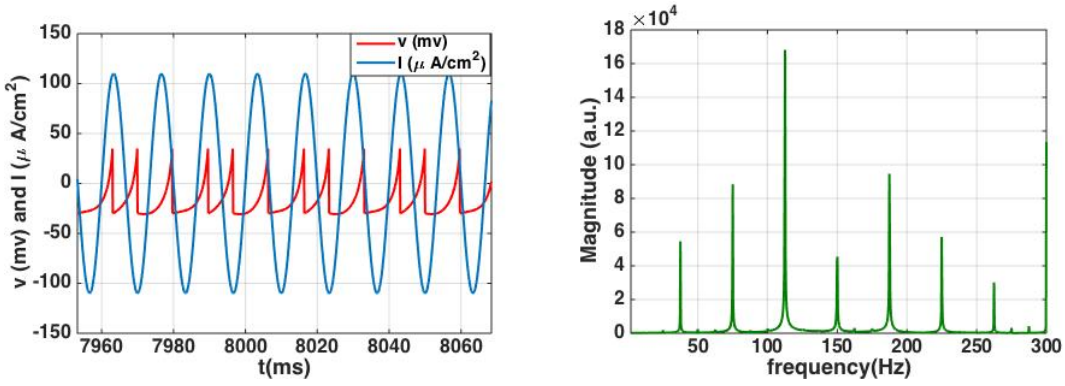

(a) (b)

Figure 1.6: 1^{st} example, $3:2$ mode-locked pattern (a) Time series diagram of a sinusoidal stimulus with amplitude of $A = 120\mu A/cm^2$ and frequency of $f = 75Hz$(blue) and the corresponding spike pattern (red) (b) Frequency spectrum of the spike pattern corresponding to a sinusoidal stimulus with amplitude of $A = 110\mu A/cm^2$ and frequency of $f = 75Hz$.

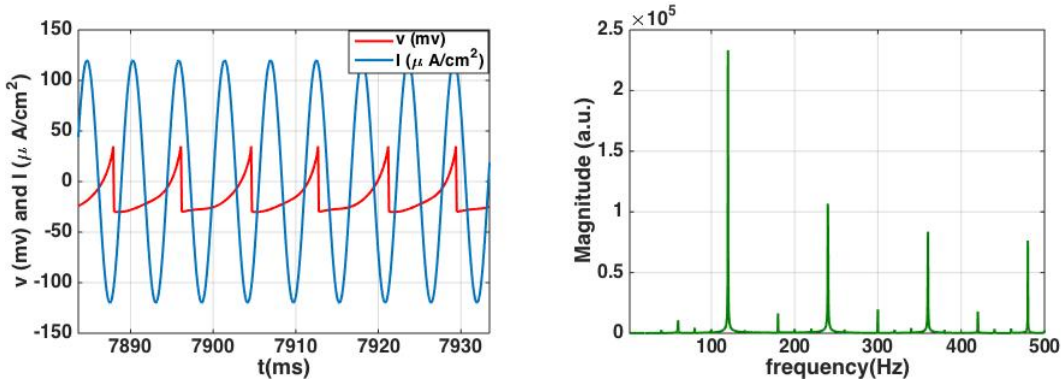

(a) (b)

Figure 1.7: 2^{nd} example, $2:3$ mode-locked pattern (a) Time series diagram of a sinusoidal stimulus with amplitude of $A = 120\mu A/cm^2$ and frequency of $f = 180Hz$(blue) and the corresponding spike pattern (red)(b) Frequency spectrum of the spike pattern corresponding to a sinusoidal stimulus with amplitude of $A = 120\mu A/cm^2$ and frequency of $f = 180Hz$.

or supercritical Andronov-Hopf bifurcation, i.e. the neuron acts similarly to a bandpass filter in that it extracts the frequencies which correspond to resonant frequencies. This information can be related to our observations and help explain

why sub-harmonics formation in Class-2 neurons can be more dominant than in Class-1 neurons. The firing frequencies give in F-I curves (Fig. 1.1) depend on factors beside the type of bifurcation of the resting state. Particularly low-frequency firing can be observed in class-2 neurons [12]. Neurons that undergo Hopf bifurcation show damped oscillations, while the ones that undergo saddle node bifurcation on or off an invariant circle do not exhibit such oscillations. The small amplitude oscillations make the neurons to resonate to the driving frequency.

1.3.3 Computing Arnold tongues based on vector strength

The methods used in the above analysis work well for a deterministic model, however they begin to break down when noise is applied to the model. We use the spiking model of Izhikevich, including threshold and additive noises $\xi(t), \zeta(t)$ and $\eta(t)$ respectively:

$$\begin{cases} C\dot{v} = k(v - v_r + \zeta(t))(v - v_t + \xi(t)) - u + I_{DC} + I_{AC} + \eta(t) \\ \dot{u} = a[b(v - v_r) - u] \\ if \quad v \geq v_{peak} \quad then \quad v \longleftarrow c \ , \ u \longleftarrow u + d \end{cases}$$

In addressing this more realistic situation we consider vector strength (VS). As mentioned previously, VS takes on a value near 1 when the neuronal spike events always occur at the same phase of the stimulus and vanishes for equally distributed spike times.

The vector strength quantifies the amount of periodicity in a neuronal response to a given periodic signal. The neuronal response is denoted by a sequence of spike times $\{t1, t2, ..., tn\}$ where in general $n \gg 1$. t_j is defined for $1 \leq j \leq n$. VS is the

length of the synchrony vector[36]:

$$VS = \frac{1}{n}|\sum_{j=1}^{n} e^{-i\omega t_j}| \tag{1.4}$$

Here, $\omega = \frac{2\pi}{T}$ denotes an angular frequency for some period T. Eq.(1.4) transforms the spike times t_j, or more precisely the dimensionless times t_j/T onto a circle with radius 1.

As previously mentioned, deterministic computation we introduced in the previous sections cannot be utilized in the presence of noise. The advantage of using VS based Arnold tongues is that it can be used for noisy model. However there exists a fundamental problem that VS can only be used to analyze $1:1$ mode-locking[35]. Nevertheless, we suggest an idea that lets us extend this method to all mode-locked states by considering the pattern existence, i.e. to use Eq. 1.4 by substituting the time of the first spike per period. Using VS in this way is akin to 1:1 mode-locking analysis, and can be done by looking at the interspike interval scattergrams.

Interspike intervals ($ISI = t_{j+1} - tj$) can be plotted successively so that they form ISI scattergrams. Figs.(1.8) and (1.9) show some examples of ISI scattergrams for different mode-locked states and their corresponding spike trains. If the model is deterministic (no noise) the clusters in ISI scattergrams shrink to number of points corresponding to the n number of spikes per m periods of stimulus. In the presence of noise, however, there tends to be clusters of points bound in regions around the deterministic points. The boundaries around these points can be defined in a way that yields the area of clusters depending on the level of noise. This allows us the compute the mode-locked regions in the presence of noise. The smaller the cluster the bigger VS and consequently the higher stability

of the mode-locked strength.

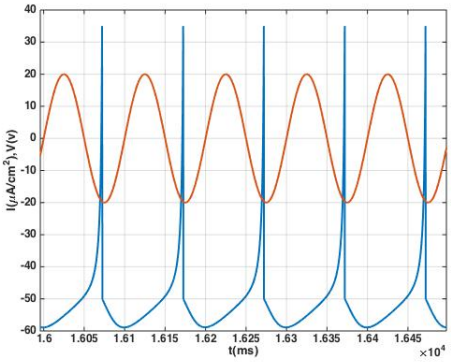

(a) 1:1 mode-locked state spike trains

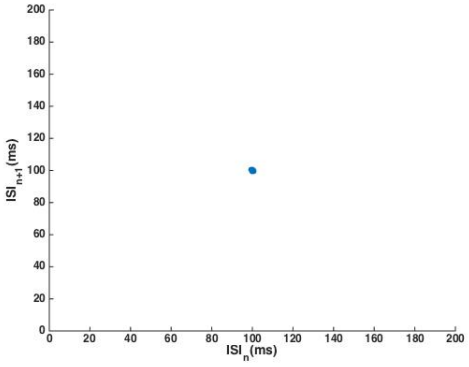

(b) 1:1 mode-locked state ISI scattergram corresponding to (a)

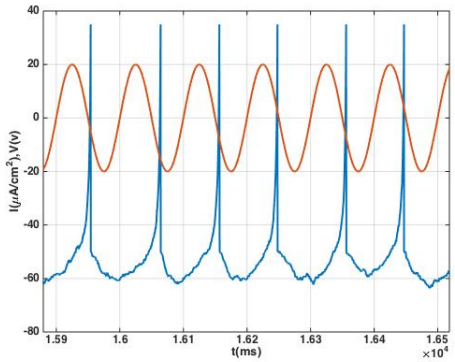

(c) Still 1:1 mode-locked but with less stability

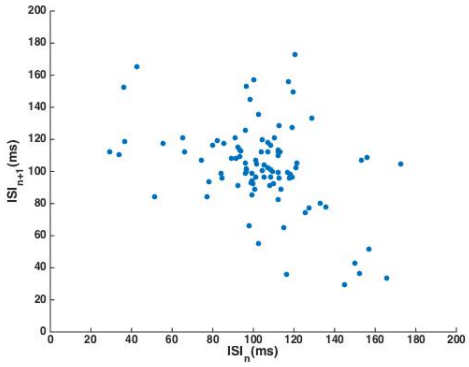

(d) Noisy ISI scattergram corresponding to (c)

Figure 1.8: An example of a 1:1 mode-locked state without noise (a) spike trains and (b) the correspoding ISI scattergram. After adding the white Guassian noise with $\mu = 0$ and $\sigma^2 = 5$ (c) the mode-locking pattern becomes less stable and the corresponding ISI scattergram (d) is not a well defined point anymore.

The number of clusters tells us the denominator of the mode-locking ratio. We chose only one of the clusters, and then measured VS over the whole time of recording only for that cluster. The method to choose the preferred cluster in ISI scattergrams is analogues to select the preferred phase around a mean value on a

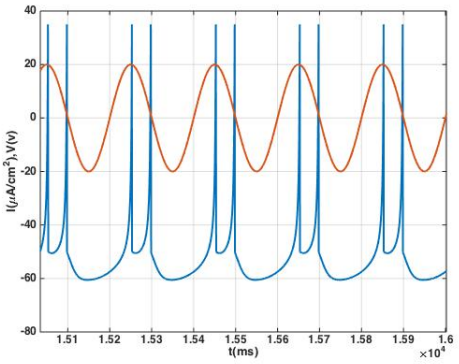

(a) 2:1 mode-locked state spike trains

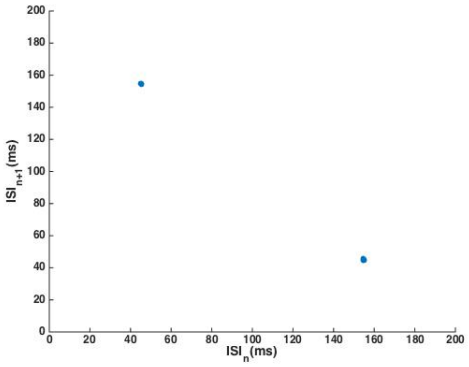

(b) 2:1 mode-locked state ISI scattergram without noise

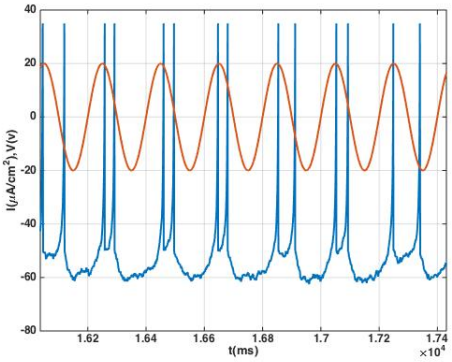

(c) Still 2:1 mode-locked but with less stability

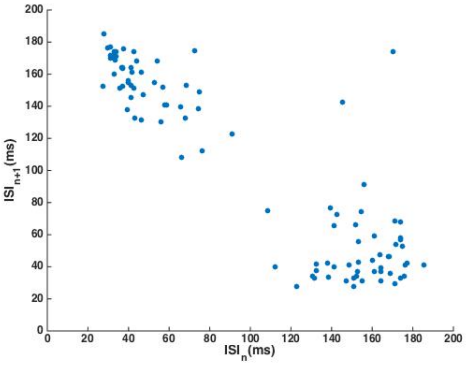

(d) 2:1 mode-locked state ISI scatergram with noise

Figure 1.9: An example of a 2:1 mode-locked state without noise (a) spike trains and (b) the correspoding ISI scattergram. After adding the white Guassian noise with $\mu = 0$ and $\sigma^2 = 5$ (c) the mode-locking pattern becomes less stable and the corresponding ISI scattergram (d) is not two well defined points anymore.

circle defined by a radius that its magnitude is equal to VS. Fig. 1.10 shows the phase analogue of the ISI scattergram in Fig. 1.9d. We find the mean value of the smaller angle ϕ, which corresponds to the center of one of the clusters by $\phi = \omega t$ and choose a window $\delta\phi$ that is defined by user. This $\delta\phi$ is related to the radius of

the already chosen cluster by $\delta\phi = \omega\delta t$. Note that we are allowed to do this since the relationship between the angle ϕ and time t is linear. In this case, even under noisy conditions there will still be synchronization, albeit with less stability than the deterministic model.

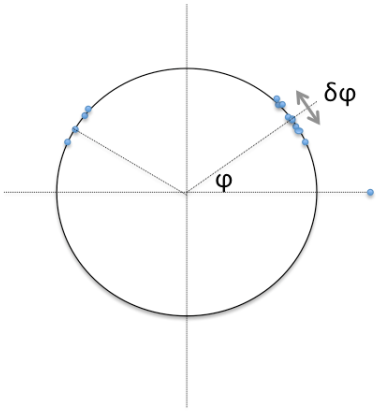

Figure 1.10: Unit circle that is used to find the smallest phase, ϕ. The window $\delta\phi$ is defind by user and indicates the radius of the cluster under study in the ISI scattergram, Fig. 1.9d.

Fig.(1.11) illustrates the evaluated Arnold tongues based on VS concept for class-1 neuron both with and without noise. In the same fashion we obtained VS based Arnold tongues for class-2 neuron in Fig.(1.12). It can be seen that the deterministic VS based Arnold tongues (Figs. (1.11a) and (1.12a)) confirm Figs. (1.2) and (1.5) as having the same shape and structure. The boundaries of different mode-locking regions are the same. In the presence of noise (Figs. (1.11b) and (1.12b)), it is observed that the tongues edges (boundaries) become less distinct and some of the tongues (e.g. $5:4$) completely disappear. In this process it appears that the tongues corresponding to $n:m$ mode-locked states with $n > m$ are more stable than those with $n < m$.

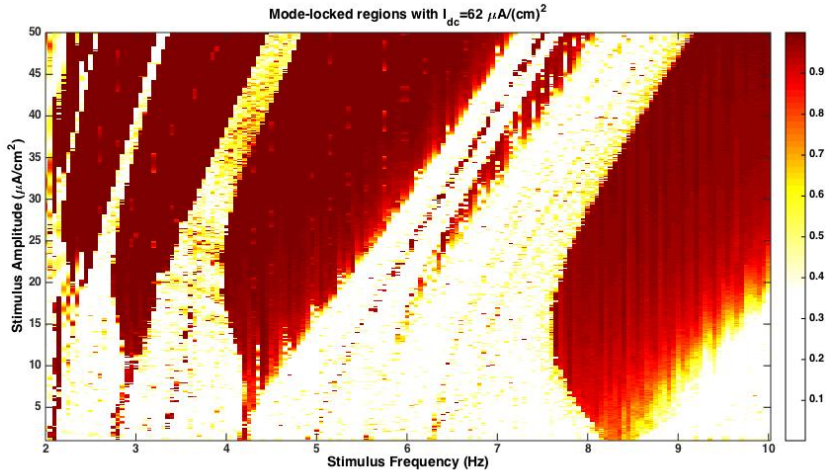

Figure 1.11: VS based Arnold tnguea diagram of a class-1 neuron in the presence of noise. Time step for computing the Izhikevich model is $dt = 0.05ms$. The color code represents the amount of vector strength. Note how the different mod-locked states lose their stabilities with the addition of noise compared with Fig. 1.2.

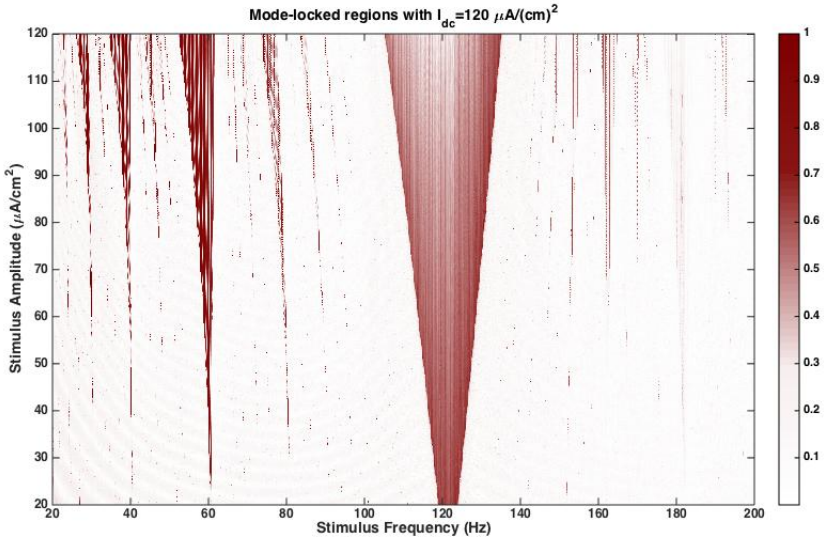

Figure 1.12: VS based Arnold tnguea diagram of a class-2 neuron in the presence of noise. Time step for computing the Izhikevich model is $dt = 0.05ms$. The color code represents the amount of vector strength. Note how the different mod-locked states lose their stabilities with the addition of noise compared with Fig. 1.5.

1.4 Conclusion

Using Izhikevich neurons, we have constructed a deterministic model which simulates the mode-locking of a single neuron to external sinusoidal forcing. However, real neurons have noisy responses. Traditional approaches cannot be directly applied here, so we developed a novel approach using a modified vector strength method in order to account for the stochastic nature of the system. Employing this method, we constructed Arnold tongue diagrams for a stochastic system in which we examined how the presence of noise influenced the degree to which mode-locking was observed.

This is of importance because neural encoding in the auditory system is inherently noisy[4, 21, 27]. Inner hair cell (IHS) receptor potentials follow oscillatory motion, but are low-pass filtered[4, 7]. There is stochastic neurotransmitter release between IHS and auditory nerve fibers (AN) and the resulting action potentials reflect the time-varying nature of IHC membrane oscillations. AN fibers project to cochlear nucleus (CN) of the brainstem. The stellate cells in CN include choppers and onsets which differ in timing of the firing in response to periodic stimuli. This sensory coding includes mode-locking phenomenon and is also observable in higher levels of the auditory system such as inferior colliculus (IC) [3]. In order to understand and address these complex interactions, Arnold tongue diagrams of the cells aforementioned give us a global map in parameters space that could be used in justifying the observations.

Computational techniques used to investigate mode-locking have become an important tool in the analysis of synchronization. Recent investigations into periodic forcing have provided a wealth of information regarding the processing of

temporal information and the characteristics of synchronization[19, 26]. Arnold tongues and other bifurcation structures in phase space can help us explain the neuronal behaviors seen in auditory signal processing neurons such as those in the cochlear nucleus[25] and inferior colliculus.

The conclusions and methods presented here will be applied in the study of physiological data[25]. Utilizing raster plots containing spike times of neurons in response to a stimulus, we will fit the parameters of this model to period histograms produced from this data. Applying this methodology, we will construct the Arnold tongues of the particular neuron under study.

Chapter 2

Evidence of Mode-locking in Auditory System and Predictions of Arnold Tongues

2.1 Introduction

Many studies have shown that phase-locking occurs in different cell types of the auditory system. The neuronal responses to sound stimuli are not passive responses, we must consider the dynamics of the neuron and its interaction with the environment. For example Laudanski et el.(2009) showed responses that resemble mode-locked responses in different cells of the auditory system. These observations suggest that a dynamical process affects the response of neurons to a stimulus.

Here we use different sets of data to study mode-locking behavior in the auditory system. One set was recorded from rabbit inferior colliculus neurons, and the other set is from cochlear nucleus neurons in a dial-anesthetized cat. Sensitivity to AM has been investigated extensively in humans because fluctuations in amplitude represent an important form of temporal information in speech, music, and environmental sounds[6]. The inferior colliculus (IC) is a key location for studying AM coding because it is the first location in the ascending pathway where rates are tuned to AM frequency[3, 16].

Mode-locking constitutes a general description of discharge patterns synchronized to periodic stimulation. Mode-locking results from the interaction between the dynamics of a nonlinear oscillator and a periodic stimulus[25]. For example, we can think of a neuron in a given layer of the auditory system as a nonlinear oscillator, which responses to a periodic stimulus such as a tone, click train or sinusoidally amplitude modulated (SAM) stimulus. This response may be "locked" to the stimulus in terms of the mode of oscillation, i.e. the oscillation of the neuron and the corresponding spike train have the same mode, or an integer ratio of the mode, of oscillation as the stimulus. In other words a neuron is $n : m$ mode-locked

to a periodic stimulus if it fires n spikes per m cycles of the stimulus, where m and n are arbitrary integers. The locking condition reads[35]:

$$|\phi_{n,m}| < const, \tag{2.1}$$

where $\phi_{n,m}(t) = n\phi_1(t) - m\phi_2(t)$ and $\phi_{n,m}$ is the generalized phase difference, or relative phase. The definition of synchronization in noisy and/or chaotic systems is not trivial. It has been shown that the notion of phase can generally be introduced for chaotic systems as well, and phaselocking in the sense of Eq. (2.1) can be observed [32].

We make use of the Arnold tongues diagrams to help understanding the organization of the responses to SAM tones across a range of amplitudes and frequencies. Arnold tongues are regions of the parameter space (amplitude-frequency plane) that specify the stable bounded regions where the response of the neuron is locked to the stimulus for any given ratio of modelocking.

The physiological data was analyzed by producing the ISI histogram, ISI scattergram and phase histograms[25]. We shuffle the phase histograms to check the p-value of the Rayleigh test, a statistical test to test the hypothesis that the responses are due to chance. For data that passed the test, we modeled the phase histograms by fitting the parameters of the model to the recordings. Having these parameters, Arnold tongues of the model neuron are computed by using VS method decribed in chapter 1.

2.2 Methodology

Experimental Data Collection and Neural Recordings

One data set is the SAM tone responses of inferior colliculus neurons in the awake rabbit. The analysis strategy presented here was tested on the responses of an inferior colliculus neuron (IC) in the awake rabbit in response to SAM stimuli. This data set was recorded as part of a study of physiological responses to SAM stimuli, in which the methods are described in detail[3]. Briefly, extracellular recordings were made the IC using tetrodes. Single neurons were isolated by sorting spikes based on the shapes of the waveforms[33]. Acoustic stimuli were presented to the ear contralateral to the recording site using a Beyer Dynamic earphone fit to a custom earmold. Stimuli were calibrated with a probe-tube microphone (Etymotic ER-7C). The frequency to which each cell responded most strongly (best frequency, BF) was characterized using tones presented across a range of frequencies and sound levels. Then 100-modulated SAM stimuli with a carrier frequency, f_c, matched to the BF were used to identify the neuron's best modulation frequency (BMF). Finally, recordings were made with $f_c = BF$ and $f_m = BMF$ for modulation depths, m, from -30 to 0 dB (i.e. $20 \log m$).

The stimulus had a carrier frequency of $3000Hz$, which is approximately the cell's best frequency. Stimulus level was 76 dB SPL. Modulation frequency was 80 Hz sinusoidal and modulation depths ranged from -30 to 0 dB in 5 dB steps, plus "-Inf" which was the response to an unmodulated tone. In another experiment on the same cell, the stimulus level was 56 dB SPL with modulation frequency at 100 Hz having the same carrier frequency. The raster plots of the neuron under two different settings mentioned above are presented in Figs. 2.1 and 2.2.

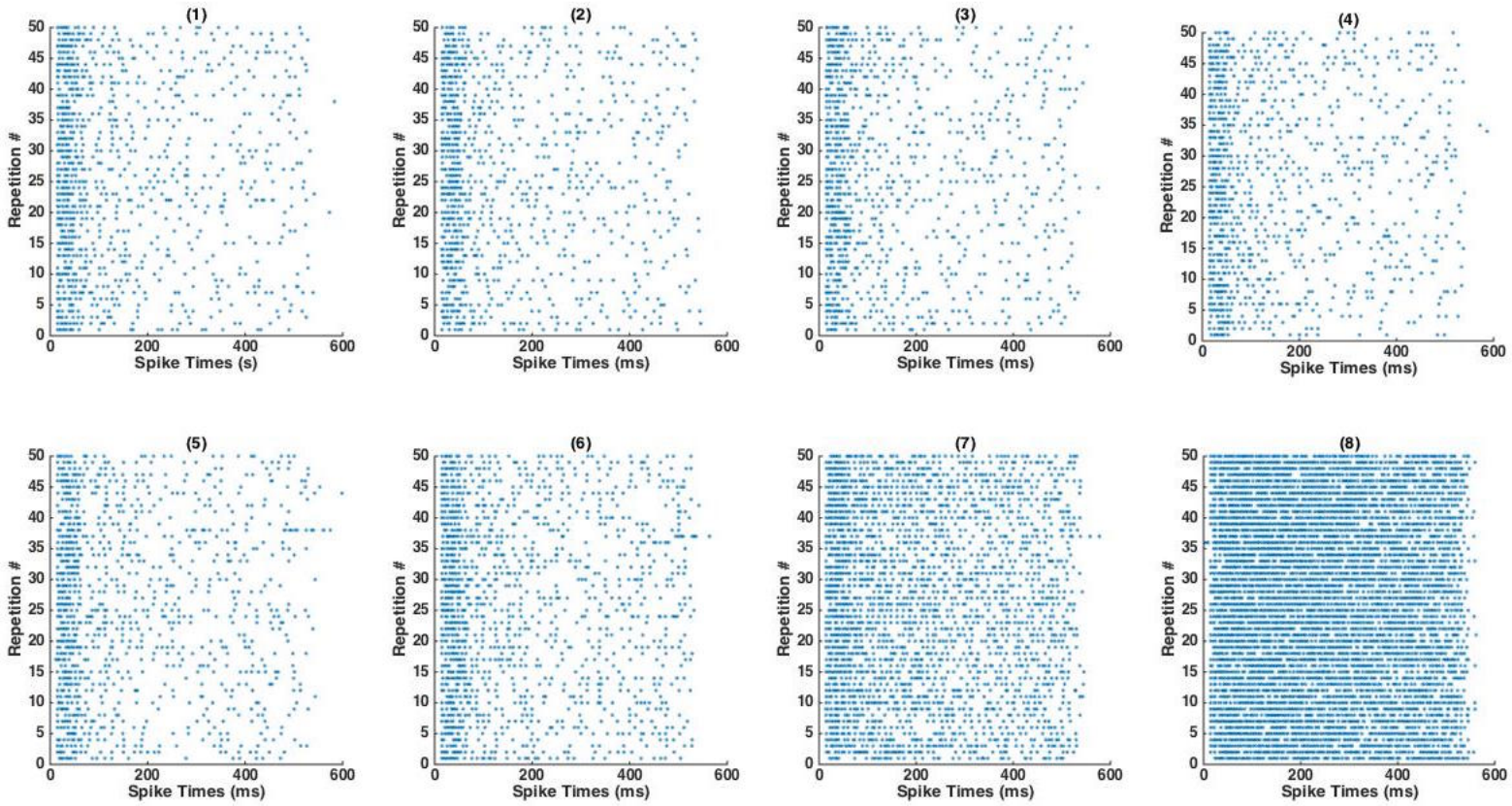

Figure 2.1: Raster plots for stimulus with sound pressur level of 76 dB, $f_m = 80\ Hz$ and $f_c = 3000\ Hz$. Raster plot (1) presents the response of the neuron for unmodulated tone (-inf modulation depth). The modulation depth at raster plot (2) is $-30\ dB$ and increases successively by steps of 5 dB in the following rasters until raster plot (8) that presents the neuron's response under full modulation, 0 dB .

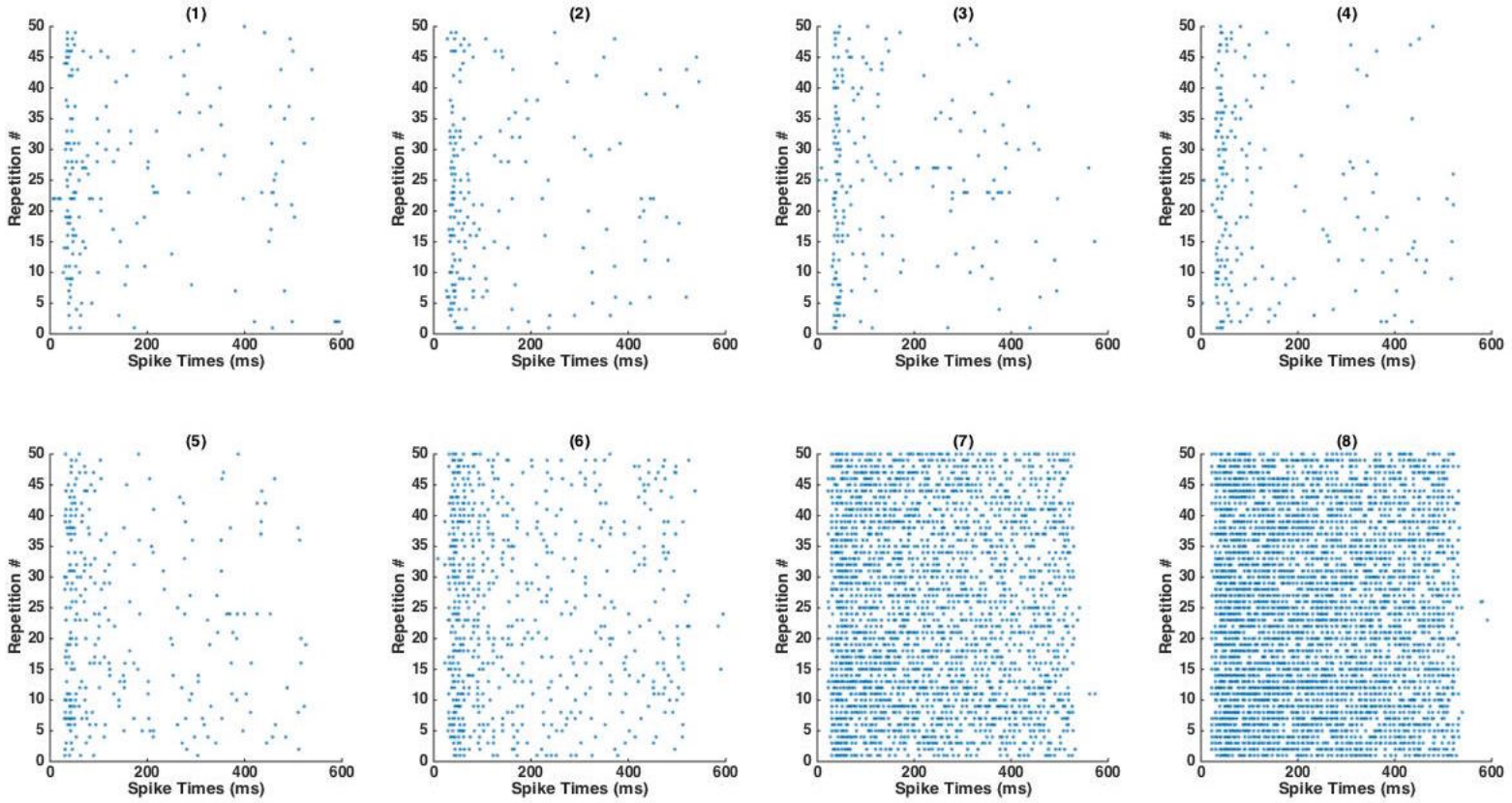

Figure 2.2: Raster plots for stimulus with sound pressur level of 56 dB, $f_m = 100\ Hz$ and $f_c = 3000\ Hz$. Raster plot (1) presents the response of the neuron for unmodulated tone (-inf modulation depth). The modulation depth at raster plot (2) is $-30\ dB$ and increases successively by steps of 5 dB in the following rasters until raster plot (8) that presents the neuron's response under full modulation, 0 dB .

Model

We used the noisy spiking model of Izhikevich explained in chapter 1, section 1.3.3.

Data Analysis

Synchronization measures:

phase histograms, vector strength and Arnold tongues

To study the mode-locking behavior of a single neuron, we must focus on phase relations between the periodic external forcing to a neuron (input) and its spike pattern (output). To address these phase relations in experiments in which sinusoidal amplitude modulated tones have been used[3, 25], we can mimic the SAM stimulus with a single sinusoidal wave at the modulation frequency, because the phase of the carrier is not changed by amplitude modulation[16]. As we described in chapter 1 with details, mode-locked spike trains can be described through their sequence of ISI, $ISI_n = T_{n+1} - Tn$ [25]. A mode-locked sequence is thus defined by a set of n phases, which repeats every mT, where T is the stimulus period. The presence of ISI patterns can be displayed using ISI scattergrams, explained in chapter 1. Because a periodic sequence of p ISIs is constituted of ordered pairs of ISIs, the sequence appears as a set of n points.

Displaying preferred ISI pairs with ISI scattergrams does not necessarily confirm mode-locking in data. Scattergrams are only useful to show that there is a well defined pattern in the spike train. However, for the spike train to be mode-locked the timing of spikes need to match *both* the phase and ISI description of mode-locked discharges. For each data set we not only constructed the ISI histograms and scattergrams, but also the phase histograms.

To analyze the synchronization of an oscillator with an external forcing, it is constructive to do the analysis such that we can obtain a global map of synchronization regions or Arnold tongues, as described earlier in chapter 1. We compute Arnold tongues in the presence of noise by computing vector strength for each amplitude and frequency of the stimulus. The advantage of using VS-based Arnold tongues is that they can be used for noisy models and data.

Importance of phase shuffling and Rayleigh statistical test

To check if the observations obtained by phase histograms are not due to chance, we use the Rayleigh statistical test. This test provides a value (P) that suggests if we are allowed to reject the null hypothesis. Null hypothesis (H_0) means the parent population is uniformly distributed (randomness). In other words, if the randomness in our data is very small and the observation is not due to chance, the value of P is very small ($P << 1$). Therefore if we shuffle the spike times that are given in the raw data they should result in a flat phase histogram, suggesting no preferred phase(s). After phase histograms are produced, we shuffle the ISI intervals and obtain a new phase histogram. If the new phase histogram has a P-value much less than the P-value of the first histogram, then we are sure that this is not a process that comes by chance[25]. Phase shuffling removes the main peaks of the histogram and produce an almost flat one.

We need to run the Rayleigh test many times to see if it always happens and that mode-locking is a unique phenomenon. In our data we repeated the test for 1000 times to assure that all the P-values after phase shuffling are greater than the critical value.

After that we confirm mode-locked responses of neurons to associated stimuli,

we use the spiking model to fit phase-histograms of data. While we find proper parameters to describe the neuron behavior throughout the fitting process, we construct the Arnold tongues of the specific neuron. This strategy is not only important to give a measure of mode-locking but also useful for prediction; after having the Arnold tongues of the neuron under study, we could guess any other possible response to an arbitrary amplitude and frequency of the stimulus.

2.3 Results and Discussion

Spike timing and mode-locking in response to periodic stimulation

In the recording described in experimental data collection section, we observe responses of an awake rabbit inferior colliculus cell stimulated by an amplitude-modulated sound with the level of 76 dB SPL, carrier frequency of $f_c = 3000\ Hz$ and modulation frequency of $f_m = 80\ Hz$, as presented in Fig. 2.1. The raster plots of the two modulation depths -5 and $0\ dB$ represented in Fig. 2.1 as number 7 and 8, are given in Figs. 2.3 and 2.4, respectively. As described in methodology section, to illustrate mode-locking since we only deal with the phase of each oscillator, we can represent the AM stimulus by a sinusoidal wave at the frequency of modulation. In Figs. 2.3 and 2.4 the corresponding sinusoidal wave at $f_m = 80\ Hz$ is presented under the neuron's raster plots.

In order to observe a pattern existence in the neuron firings, we construct a peristimulus time histogram (PSTH) that shows the number of firings for each period of stimulus vs. time given in Figs. 2.5 and 2.6 (bottom left corner). One can observe that most of the firings happen in a $2:1$ fashion, meaning that for each period of the AM there are two neuron firings. However, this does not necessarily

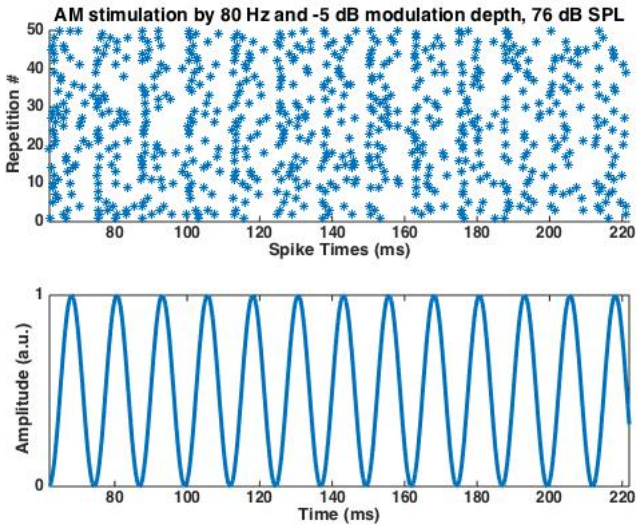

Figure 2.3: Expanded raster plot and the corresponding sinusoid that represents the envelope of that SAM with a frequency $f_m = 80Hz$ and modulation depth of -5 dB with 76 dB SPL.

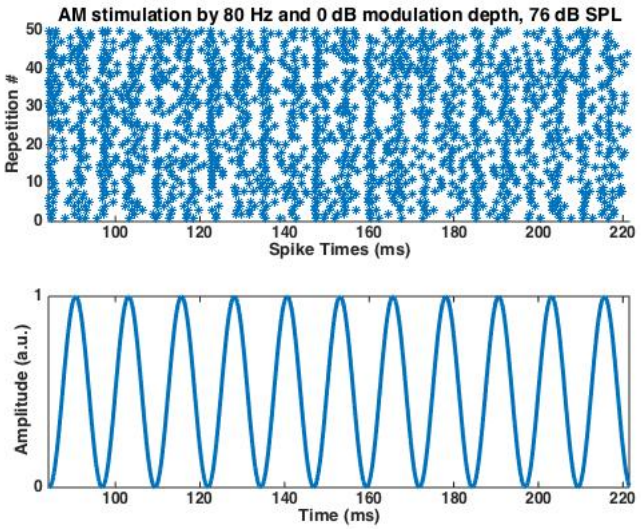

Figure 2.4: Expanded raster plot and the corresponding sinusoid that represents the envelope of that SAM with a frequency $f_m = 80Hz$ and modulation depth of 0 dB (full modulation) with 76 dB SPL.

mean that the phase of the neuron's spikes are locked to certain phases of stimulus. To show that there is mode-locking, we construct the ISI histograms and ISI scattergrams of the data given in Figs. 2.5 and 2.6 (middle) along with the phase histograms (top right corner). The two main clusters observed in ISI scattergram suggest the numerator of the pattern**??**, which in this case is 2, but cannot tell us anything about the denominator. We still need another statistical tool that shows the pattern is locked to the stimulus and is not changing over periods of stimulus oscillations (mode-locking phenomenon). This is done by obtaining the phase histogram of the data, Figs. 2.5 and 2.6 (top right corner). The advantage of the phase histogram (period histogram) is that it shows the number of firings that happen at a certain phase over the stimulus duration.

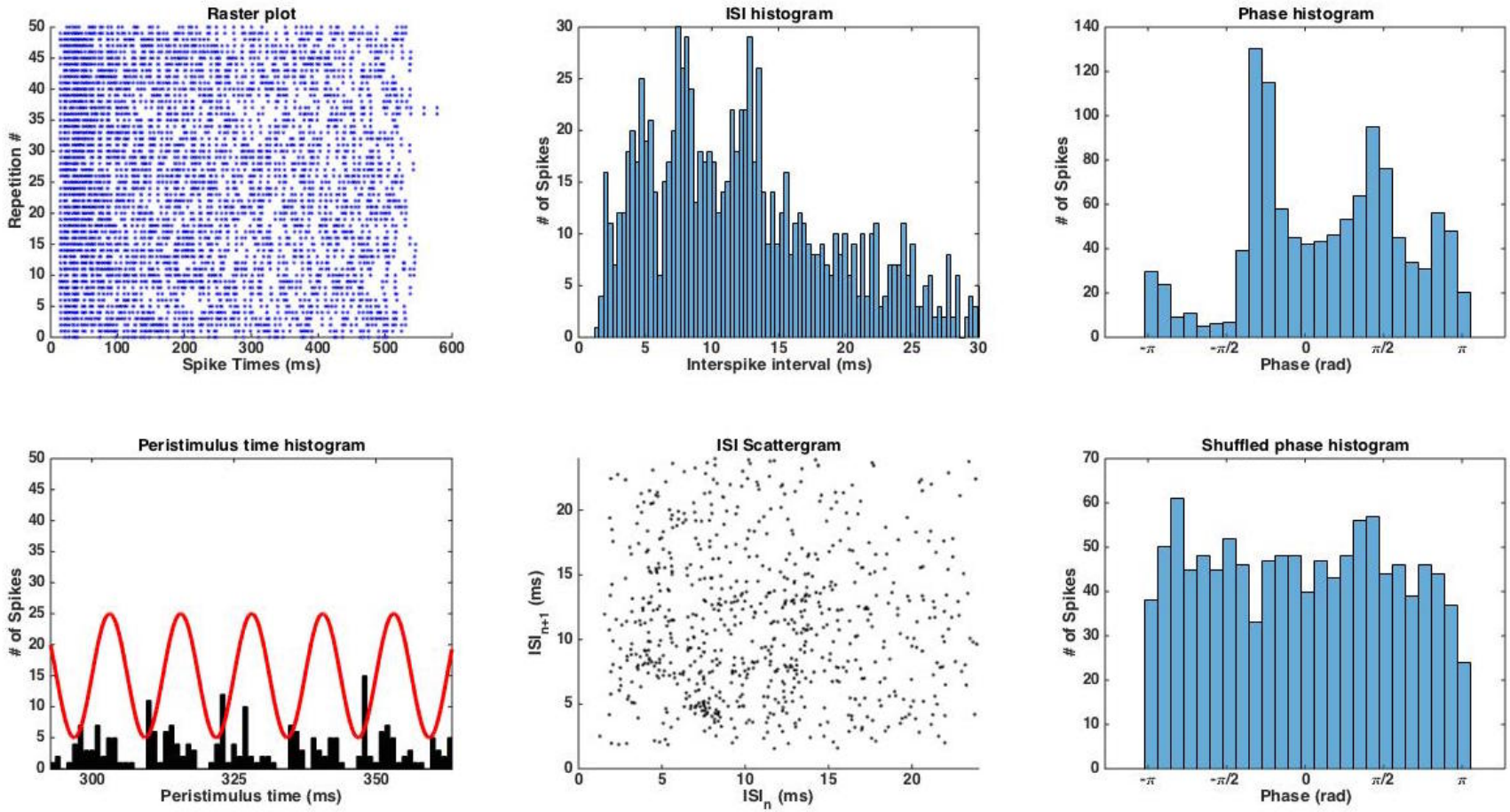

Figure 2.5: Raster plot, PSTH, ISI histogram, ISI scattergram, phase histogram and shuffled phase histogram for the level of 76 dB SPL and -5 dB modulation depth.

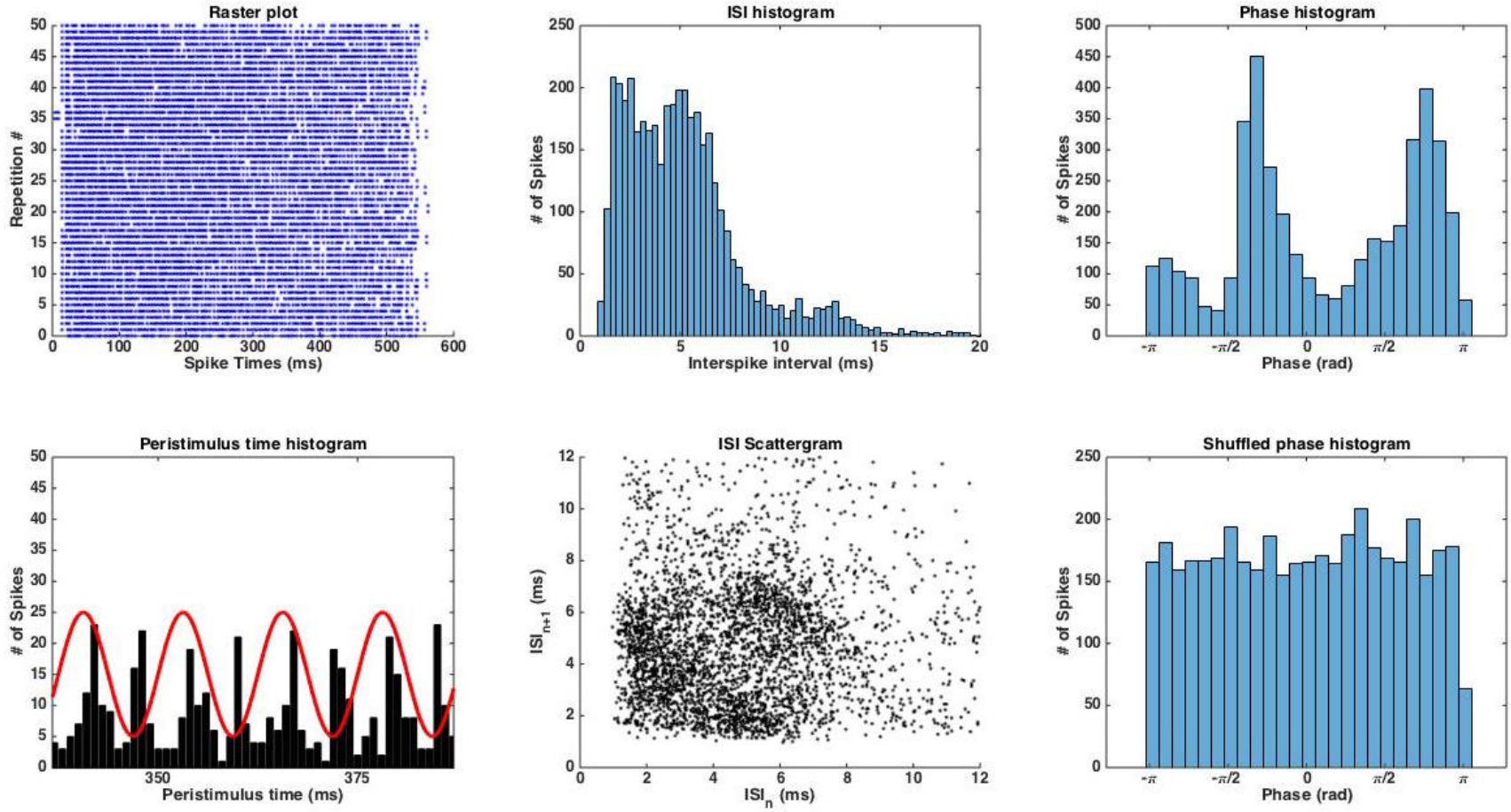

Figure 2.6: Raster plot, PSTH, ISI histogram, ISI scattergram, phase histogram and shuffled phase histogram for the level of 76 dB SPL and 0 dB modulation depth (full modulation).

Mode-locking criteria, test of randomness

The blue histogram in Fig. 2.7 is the initial phase histogram and the green one is obtained after shuffling the spike times. One can see the preferred phases disappear after shuffling the spike times. By using MATLAB circular statistics toolbox[1] the P-value of the test before shuffling is computed to be $P = 1.6539 * 10^{-6}$. After shuffling, this value becomes much higher, $P_s = 0.4986$, suggesting the randomness and uniformity of the phase distribution.

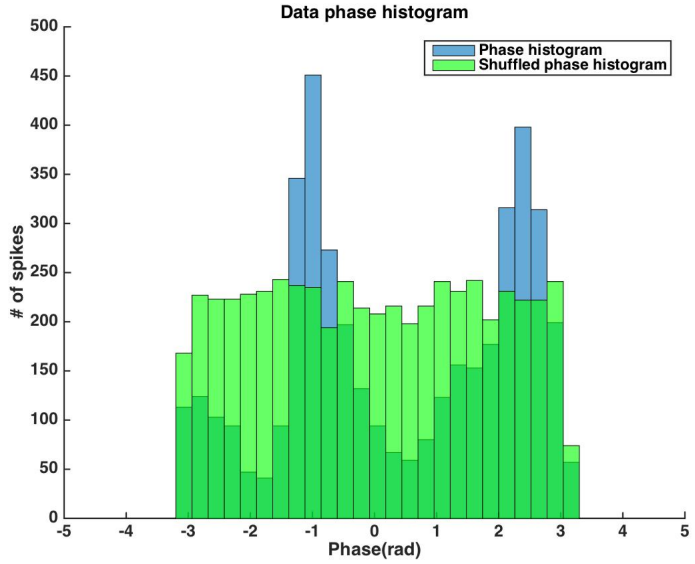

Figure 2.7: P-value of data is $P = 1.6539 * 10^{-6}$ and P-value after phase shuffling is $Ps = 0.4986$.

We do the Rayleigh test 1000 times and the average of the P-values after all phase shufflings is $\bar{P}_s = 0.68$. The results are shown in Fig.2.8 along with two critical values $a = 0.05$ and $b = 0.025$. There is only one P_s less than a and no observation of P_s less than b, which means the test of randomness is successful.

This shows that $2:1$ mode-locking happens in our data, the neuron's response pattern is $2:1$ locked to the envelope of the SAM stimulus.

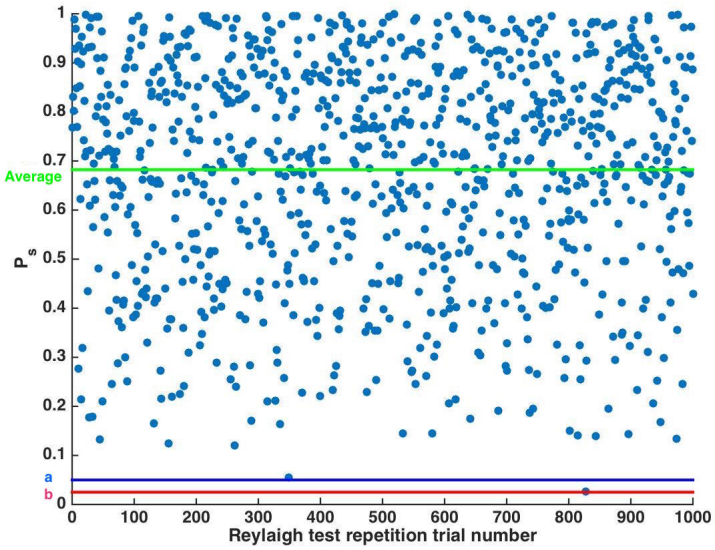

Figure 2.8: The first critical value is set as $a = .05$ (blue line) and the second one is set as $b = 0.025$ (red line). The average of the P-values after shuffling is given by the green line ($\bar{P}_s = 0.68$). All the P-values afer shuffling pass the test as they are not lower than the critical value, (b) .

Fitting data phase histogram with the model

Referring to the noisy model introduced in chapter 1, we see there are number of parameters we need to set for the neuron under study. Some are neuron parameters and the others are stimulus parameters. Starting from stimulus parameters we have I_{DC}, I_{AC} and f. We know that $f = f_m$. So the there remains I_{DC} and I_{AC}. The phase histogram suggest 2:1 locking, which means the firing rate of the neuron should be around twice of f_m, which is about $160Hz$. Referring to Figs. 1.1 we see that the cell belongs to class-2 category as to have $f = 2f_m$ it requires $I_{DC} = 220.4$ which cannot be handled by a class-1 neuron. So we set the values of the neuron parameters equal to a fast spiking neuron suggested by Izhikevich[12]. For I_AC we try to chose it within a limit that does not change the firing rate of the neuron, by referring to Fig. 1.1b. We found it by try and error to be 5.3. Now

the only remaining parameters are the noise parameters η, ζ and ξ. The additive noise η does not alter the model phase histogram dominantly, so it could be fixed. The only remaining variables are then ζ and ξ.

We define the vector x as a vector that contains the parameters of the model neuron to be evaluated by the fitting process. In order to find the best model neuron parameters that could describe the given data, we minimize the difference between the area under the smoothed fits of the data and model phase histograms, i.e. minimizing the error described by the integral below:

$$x^* = arg\min_x \| \int_{-\pi}^{\pi} [S_{model}(\phi) - S_{data}(\phi)] \; d\phi \; \|, \tag{2.2}$$

where $S_{data}(\phi)$ and $S_{model}(\phi)$ are the smoothed fits of the data and model phase histograms respectively. x^* is a vector that contains the parameters we are looking for to minimize the given integral. Note that in our case $x = [\zeta, \xi]$ as we set the other model parameters fixed, described above.

We minimized the fitting error by using the fminsearch routine in MATLAB. This tool finds the minimum of a scalar function of several variables, starting at an initial estimate. This is generally referred to as unconstrained nonlinear optimization. The fitting result is shown in Fig. 2.9.

Arnold tongues

The model parameters found from the fitting process can be used to construct the Arnold tongue diagram of the model cell, given the amplitude of direct current injection I_{DC} that was found to be $220.4(\mu A/cm^2)$.

For each element of the amplitude-frequency matrix that forms the plane, we simulate the model for 10 seconds and then we compute VS as described in data

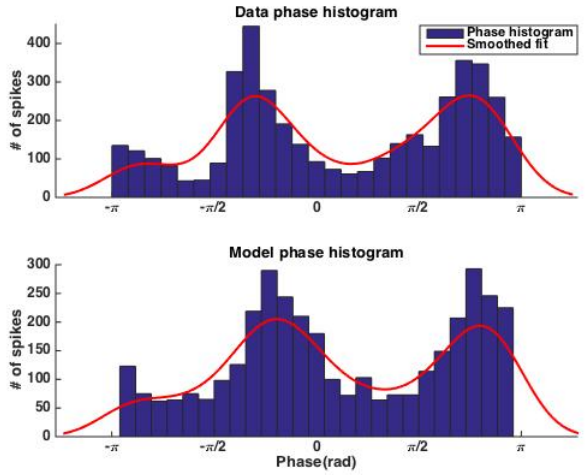

Figure 2.9: The best fit of the model to the given data was for the parameters $a = 0.1, b = 2, c = -30, d = 100, v_r = -60, v_t = -40, v_{peak} = 35, k = 0.7, C = 100$, having $I = 220.40 + 5.3\ sin(2\pi 80t)(\mu A/cm^2)$. The smoothed best fit of the model phase histogram compared with the data phase histogram kernel fit. The minimized error is $Error = 0.020$. The level of additional white Gaussian noise is $\eta = 2.2$. The amount of threshold whith Guassian noise is $\xi = 0.135$ and $\zeta = 0.2$.

.

analysis section and chapter 1. Fig. 2.10 shows the regions of the amplitude-frequency plane where different mode-locking ratios can be observed. This plot represents the mode-locked regions as a function of the amplitude and frequency of the sinusoidal forcing, with the direct current of $I_{DC} = 220.4\mu A/cm^2$. It can be seen that the element corresponds to $A = 5.3(\mu A/cm^2)$ and $f = 80Hz$ falls in $2:1$ mode-locked region, as expected by our previous data analysis.

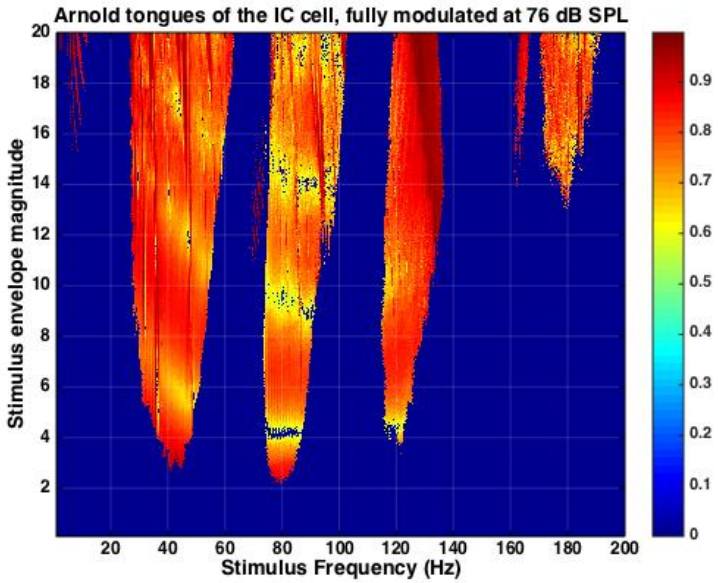

Figure 2.10: Arnold tongues diagram of the modeled neuron. The color bar indicates the amount of VS.

In this chapter mode-locking was observed in an awake rabbit IC neuron and confirmed by the described statistical tests. The confirmed mode-locked state of the neuron falls within the 2 : 1 locking region suggested by the corresponding Arnold tongues of the model neuron. Constructing Arnold tongues is a useful method to predict the other mode-locked regions so that investigators could speculate the behavior of the neuron with respect to periodic external stimuli.

Chapter 3

From Wilson-Cowan to Canonical Model: Analysis of single and Two Coupled Neural Oscillators

3.1 Introduction

Wilson-Cowan model is a model of neural oscillations based on excitatory and inhibitory neural populations. Neurons are called excitatory if they increase the probability of a postsynaptic action potential occurring, and inhibitory if they decrease this likelihood.

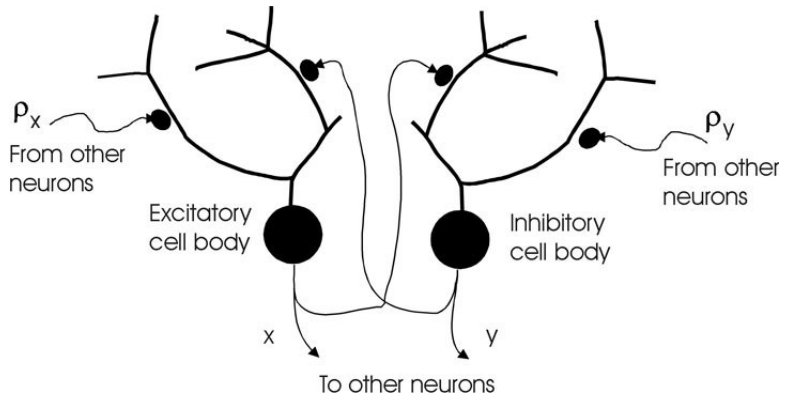

Figure 3.1: A schematic representation of a Wilson-Cowan osciallator which consists of a pair of excitatory and inhibitory neurons[29].

According to Hugh D. Wilson and Jack D. Cowan, all nervous processes of any complexity are dependent upon the interaction of excitatory and inhibitory cells [38]. The original model was introduced by Wilson and Cowan in their 1973 paper[38]. Consider an interconnected pair of excitatory and inhibitory neurons as in Fig. 3.1. Each unit in the oscillator represents a local population of neurons, in cerebellum, olfactory cortex, and neocortex. This pair is called Wilson-Cowan neural oscillator, one of the basic mechanisms of the generation of oscillatory activity in the brain[11].

Dynamical system theory is the study of time evolution given by systems of differential equations. The typical focus of the theory is not to solve the differential

equations for general initial conditions, but to study the qualitative behavior. In general they focus on *bifurcations*.

In order to make these terms more understandable, we present some physical analogies. Stability is a fundamental property of a dynamical system, which means that the qualitative behavior of its time evolution is not affected by small perturbations of the trajectory. So, equilibrium phases of thermodynamics corresponds to fixed-points in the dynamics and phase transitions corresponds to bifurcations[34]. Analysis of the transition between states in dynamical models is called bifurcation analysis[37]. Bifurcation analysis is the mathematical term analogous to abrupt and continuous or first and second order phase transitions in physics, particularly statistical mechanics. For example bifurcation parameter is defined as a parameter in a system of differential equation(s) that by changing its value, the system undergoes a qualitative change in its behavior. This is similar to the order parameter in statistical mechanics. A good example can be liquid-gas transitions in studying the phase of materials.

Complex systems can undergo transitions between different dynamical states, especially close to the transition point, show low-dimensional behavior, i.e. even though the system has many degrees of freedom its dynamics can be modeled by a set of a few nonlinear ordinary differential equations[8]. In fact, complex systems can be modeled on different levels and it is sometimes even possible to derive the dynamics on a higher (typically more abstract or microscopic) level of description. In many cases, particularly when transitions between macroscopic patterns occur, the description can be reduced to a low dimensional set of nonlinear ordinary differential equations[8].

A canonical model is the simplest (in analytical terms) of a class of equivalent

dynamical models, and can be derived using either normal form theory or centre manifold theory. The canonical model we introduce in Eq. (3.4) was derived, using normal form theory, from the Wilson-Cowan model of the interaction between excitatory and inhibitory neural populations[20, 38].

Our goal in this chapter is to produce this derivation by following step-by-step calculations and showing all the mathematical proves. However, the canonical model is generic, so it could also be derived from other models of nonlinear oscillation, including outer hair cell models[17]. Outer hair cells are responsible for the cochlea??s extreme sensitivity to soft sounds, excellent frequency selectivity and amplitude compression. The canonical model uncovers universal properties, making predictions that hold under a rather general set of assumptions[11]. This makes the canonical model especially attractive from the point of view of modelling human perception and behavior[22].

3.2 Models and methodology

Wilson-Cowan Model

Letting x_i and y_i denote activity of i^{th} excitatory and inhibitory neurons, respectively, Wilson-Cowan neural model has the form:

$$\begin{cases} \mu_x \dot{x_i} = -x_i + (1 - \tau_x x_i) S(\rho_{x_i} + \sum_{j=1}^{n} a_{ij} x_j - \sum_{j=1}^{n} b_{ij} y_j) \\ \mu_y \dot{y_i} = -y_i + (1 - \tau_y y_i) S(\rho_{y_i} + \sum_{j=1}^{n} c_{ij} x_j - \sum_{j=1}^{n} d_{ij} y_j) \end{cases} \tag{3.1}$$

where μ_x,$\mu_y > 0$ are the membrane time constants (the time needed for neurons' voltage level to decay to their resting state) and τ_x,τ_y are refractory periods (the

time needed for neurons to get opened again after the last ion transition) of excitatory and inhibitory neurons, respectively. a_{ij}, b_{ij}, c_{ij}, $d_{ij} > 0$ for $i \neq j$ are synaptic coefficients. b_{ii} and c_{ii} are synaptic too, since they denote interactions between excitatory and inhibitory neurons within the i^{th} neural oscillator.a_{ii} and d_{ii} are feedback parameters, which can be positive or negative. Parameters ρ_{x_i} and ρ_{y_i} denote the external input from sensory organs and other regions of the brain to the i^{th} excitatory and inhibitory neurons respectively. S is a function with sigma shape that is continuous, monotone increasing and satisfies $S(-\infty) = 0$, $S(+\infty) = 1$. For simplicity, we consider the Wilson-Cowan neural model in the special case $\tau_x = \tau_y = 0$, i.e. ion channels open immediately and $\mu_x = \mu_y = 1$. That is:

$$\begin{cases} \dot{x_i} = -x_i + S(\rho_{x_i} + \sum_{j=1}^{n} a_{ij}x_j - \sum_{j=1}^{n} b_{ij}y_j) \\ \dot{y_i} = -y_i + S(\rho_{y_i} + \sum_{j=1}^{n} c_{ij}x_j - \sum_{j=1}^{n} d_{ij}y_j) \end{cases} \tag{3.2}$$

Normal Form Theory

Next we use the method of *normal form theory* to reduce the dimensions of the Wilson-Cowan model to our canonical model which has just been described.

Normal form theory is one of the two approaches that mathematicians apply to simplify dynamical systems. The other one is *centre manifold theory*. Both of these approaches utilize reducing the dimensions and eliminating the nonlinearity up to the desired order. The method of normal forms can be traced back to the Ph.D. thesis of Poincaré[1929][37]. Normal form theory is one of the most powerful tools for the study of non-linear differential equations, in particular, for stability and bifurcation analysis[39]. The method of normal form provides a way

of finding a coordinate system in which a dynamical system takes the simplest form. Amazingly the structure of the normal forms determined entirely by the nature of the linear part of the vector field or say the differential equation. Computation of normal forms has been restricted to systems which do not have perturbation parameters (unfoldings)[39]. Here we apply Conventional Normal Form theory (CNF) which uses an independent non-linear transformation (that is called: near identity change of variables) to each order. This strategy is based on the fact that changing the coordinates must not affect the stability of the origin. In fact, we will use only coordinate changes that map the origin to itself.

According to local dynamical systems theory (LDS), near the origin the terms of low degree are dominant, so these are the terms which determine the behaviour of the system around the fixed point, in our case, the origin. This is not true for the points far from the origin since at those points the higher order terms are dominant. So we will be interested in the points in the vicinity of the origin, since we are going to work with the simple transformed model which is obtained by the normal form method, the method which has these features [37]:

1- Locality: the coordinate transformations are generated in a neighbourhood of the fixed point.

2- Nonlinear transformation: In general the coordinate transformation will be nonlinear functions of the dependent variables.

3- Dominance of the linear part: The sturcture of the normal form is determined entirely by the nature of the linear part of the vector field.

We can address the problems for normal form as *description* and *computation* problems. In the first, one only describes the simplest form to which any arbitrary system can be reduced and in the latter, one carries out the necessary computations

to simplify the system. Here we do both. Most of the in-depth calculations are presented in the appendices.

Canonical Model

A canonical model of Wilson-Cowan model is derived step by step in section 3.3. This canonical model facilitates the study of non-linear time-frequency transformation, which is very important in auditory signal processing[20]. The canonical model is described by the differential equation below:

$$\dot{z} = z(\alpha + i\omega + \beta|z|^2) + x(t) + \mathcal{O}(z^5) \ . \tag{3.3}$$

where z is the complex state variable that describes the state of the oscillator under study, α is the linear damping, β is the non-linear damping parameter and is negative, preventing the amplitude from blowing up when $\alpha > 0$, ω is the radian frequency and $x(t)$ is a linear external forcing as a function of time. For the case of single oscillator that we are going to discuss in more detail in section 3.3, the canonical model described by Eq. (3.3). Without considering terms of order higher than cubic becomes:

$$\dot{z} = (\alpha + i\omega)z + \beta z^2\bar{z}. \tag{3.4}$$

Here α acts as a bifurcation parameter for the system which can be either positive or negative valued. It is easy to verify that our bifurcation point is $\alpha = 0$. In order to understand the derivation of canonical model and particularly the so-called Hopf normal form out of Wilson-Cowan model we need to apply and use some important mathematical theorems.

Poincaré-Andronov-Hopf normal form

In the absence of stimulation i.e. $x(t) = 0$ in Eq. (3.3), a nonlinear oscillator can display two qualitatively different stable states, both of which depend upon the specific value of the bifurcation parameter, α. The transition between a stable equilibrium and a stable limit cycle is called Poincaré-Andronov-Hopf bifurcation. When $\alpha < 0$ the system behaves as a damped oscillator, but when $\alpha > 0$ (negative damping) the system generates a spontaneous oscillation. $\alpha = 0$ is the bifurcation point (also referred to as the critical value of the parameter), the value at which behavior changes from damped to spontaneous oscillation or vice versa. Other kinds of bifurcations that also lead to spontaneous oscillation can be found in this canonical model[9]. Models of neural oscillation often assume spontaneous activity, i.e., $\alpha > 0$. Models of cochlear outer hair cells assume critical oscillation, i.e. $\alpha = 0$, which is based on Hopf bifurcation normal form. It is proposed that, in the mammalian cochlea, the basilar membrane is driven by a set of critical oscillators (most likely identified with outer hair cells) and propagates an active traveling wave and the two-tone response of a critical Hopf oscillator has considerable bearing on human psychoacoustics [5].

Method

In this paper, we start off the *translated* Wilson-Cowan model and will obtain its conventional normal form for a single oscillator. We will see that the conventional normal form is universal and the Hopf bifurcation emerges out of it and makes the canonical model. The brain, of course, exhibit other behaviours than Hopf bifurcation. In other words this conventional normal form has the potential of

non-Hopf bifurcations and can be used in a desired format, i.e. one can keep or eliminate the higher order terms as long as desired. In this sense this CNF becomes very powerful since it can describe other kinds of bifurcations.

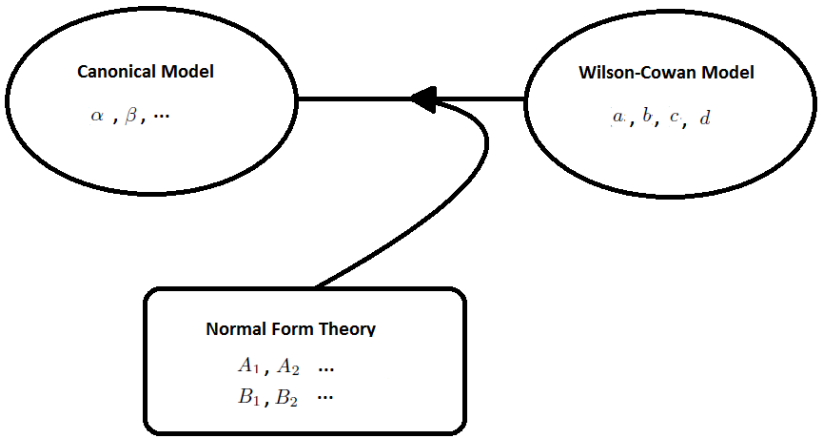

Figure 3.2: A demonstration which shows the underlying idea of this paper.We have made use of the normal form theory to reach the canonical model from the Wilson-Cowan model for excitatory and inhibitory neurons. The parameters which describe each model has been shown, too.

In section 3.4 we do the same process we did in section 3.3, but for two coupled oscillators, so we should consider not only the intrinsic properties of a single oscillator but also the coupling terms which act as an external forcing for each oscillator. Hence, the equations to describe the dynamics of the system of two coupled neurons contain extra coupling terms, and their strength and effect on the whole system can be altered by the coupling coefficient, ϵ.

Finally, in section 3.4.3 we will obtain radial and angular equations that gives us the position and phase of each oscillator on a circular plane.

3.3 Deriving canonical model for single Wilson-Cowan neural oscillator

We start by analyzing single Wilson-Cowan neural oscillator without an external input which means $i = j = 1$ (so we omit the indices) and set $\rho_x = \rho_y = 0$ in system of Eqs. (3.2).

A very good example of S is the tangent hyperbolic function since it satisfies all conditions for S. The translated Wilson-Cowan model that we start with, is :

$$\begin{cases} \dot{x} = -x + \tanh(ax - by) \\ \dot{y} = -y + \tanh(cx - dy) \end{cases} \tag{3.5}$$

To analyze the system algebraically we can expand the hyperbolic tangent function to the third or even higher orders. The first nonlinear term of the expansion for tanh function is in the third order, so we will end up with the translated Wilson-Cowan model expanded to cubic:

$$\begin{cases} \dot{x} = (a-1)x - by - ax(\frac{a^2x^2}{3} + b^2y^2) + by(\frac{b^2y^2}{3} + a^2x^2) \\ \dot{y} = -(d+1)y + cx + dy(\frac{d^2y^2}{3} + c^2x^2) - cx(\frac{c^2x^2}{3} + d^2y^2) \end{cases} \tag{3.6}$$

3.3.1 The Conventional Normal Form

In a general way we want to find the normal form of the translated Wilson-Cowan model 3.6. To this end, we should map the Cartesian coordinates on the complex domain by introducing $s = x + iy$. By differentiating s we obtain: $\dot{s} = \dot{x} + i\dot{y}$.

Now we can replace for $\dot{x}$ and $\dot{y}$ from the system of equations (3.6) to get:

$$\begin{aligned}
\dot{s} &= \dot{x} + i\dot{y} \\
&= ... \\
&= \left(\frac{a-1+ic}{2}\right)(s+\bar{s}) + \left(\frac{-1-d+bi}{2}\right)(s-\bar{s}) \\
&- \frac{a^3}{24}(s+\bar{s})^3 + \frac{b^3}{24}i(s-\bar{s})^3 \\
&+ \left(\frac{ab^2+icd^2}{8}\right)(s+\bar{s})(s-\bar{s})^2 + \left(\frac{c^2d-ia^2b}{8}\right)(s+\bar{s})^2(s-\bar{s}).
\end{aligned} \tag{3.7}$$

Note that the first two terms are linear while the rest are non-linear. We have used the fact that $x = \frac{s+\bar{s}}{2}$ and $y = \frac{s-\bar{s}}{2i}$, since we want the right hand side to be also in terms of s and its complex conjugate.

As an ansatz, we apply the near identity change of variables, i.e. to substitute s by z according to the transformation:

$$s = z + \kappa z^p \bar{z}^q. \tag{3.8}$$

where p and q are integers that their addition gives us the highest order of non-linearity present in the canonical model and κ is a complex number. This is an essential step in the normal form theory which gives us the chance to eliminate desired terms by setting appropriate value for κ, consequently simplifying the model in terms of nonlinear terms present in the expansion. Finding such value for κ is presented in appendix .1.

Rearranging Eq. (3.8) in terms of z yields:

$$\begin{aligned}
z &= s - \kappa z^p \bar{z}^q \\
&= s - \kappa(s - \kappa z^p \bar{z}^q)^p (\bar{s} - \bar{\kappa}\bar{z}^p z^q)^q \\
&= s - \kappa s^p \bar{s}^q + ...
\end{aligned} \tag{3.9}$$

If we differentiate this equation we will get an expression for $\dot{z}$. This expression without considering quintic terms and higher ($p+q=3$) is:

$$\dot{z} = \dot{s} - p\kappa s^{p-1}\dot{s}\bar{s}^{q} - q\kappa s^{p}\dot{\bar{s}}\bar{s}^{q-1}. \tag{3.10}$$

By calculations that are presented in Appendix..1 we obtain conventional normal forms of Wilson-Cowan neural model, depending on the values of p and q (either $p=1$,$q=2$ or $p=2$ and $q=1$):

$$\dot{z}_s = A_1 z + A_2 \bar{z} + A_{pq} z^p \bar{z}^q \tag{3.11}$$

with the coefficients obtained in Appendix..1. We have replaced $\dot{z}$ by $\dot{z}_s$ to show that this normal form is for a single oscillator. Note that this normal form Eq. (3.11) is capable of exhibiting all kinds of bifurcations. As an important example we will show that it exhibits a Hopf bifurcation after some simplifications and calculations which follows.

3.3.2 The Normal Form for the Poincare-Andronov-Hopf Bifurcation

In part 3.3.1 we made the transformation of the form $z \longmapsto z + h(z,\bar{z})$ where h is a third-order in z and $\bar{z}$. It is shown that[37] for some $h = z^p\bar{z}^q$ at the bifurcation point of Hopf type we must not have $p-q=-1$. This can never happen if p and q are both even numbers . Therefore all even-order terms can be removed from the expansion. For our case, we already didn't have any even order term in the expansion of tanh function, but this theorem guarantees that even if the expansion of the function S contains even order terms, they can be removed for the special

case of Hopf bifurcation. This condition also suggests us to work only with $p = 2$ and $q = 1$, so Eq.(3.11) can be written as:

$$\dot{z} = A_1 z + A_2 \bar{z} + A_{21} z^2 \bar{z}. \tag{3.12}$$

This is not the simplest normal form for the Hopf bifurcation yet. It is proved[37] that the cubic terms except $z^2\bar{z}$ can be eliminated for the Hopf normal form. This is true if and only if:

$$A_2 = \frac{a+d}{2} + \frac{1}{2} i(-b+c) = 0 \tag{3.13}$$

which means $a = -d$ and $b = c = \omega$ where ω is a real number. Substituting these results in the other coefficient A_1 leads us to:

$$A_1 = \frac{1}{2}(-2 + a - d) + i\left(\frac{b+c}{2}\right) = (a-1) + i\omega \tag{3.14}$$

By introducing $\alpha = a - 1$ and $\beta = A_{21}$, Eq. (3.12) becomes:

$$\dot{z} = (\alpha + i\omega) z + \beta z^2 \bar{z} \tag{3.15}$$

which is exactly the canonical model for single oscillator without external input under Hopf bifurcation condition we introduced in Eq. (3.4). Note that the coefficients α, β and ω are in terms of Wilson-Cowan model parameters a, b, c, d and are introduced to avoid the complexity of coefficients. The complete set of coefficients are given in Appendix..1 and one can refer to them for simulations based on canonical model. We can also confirm these results by doing stability analysis which we present next.

3.3.3 Stability Analysis

One way to find the range of the parameters in the model which represents the Hopf bifurcation is to rewrite the system in matrix form and study the Jacobian matrix. The detailed analysis is presented in this section. The linearized translated Wilson-Cowan neural model in matrix form is as below:

$$\begin{pmatrix} \dot{x} \\ \dot{y} \end{pmatrix} = \begin{pmatrix} a-1 & -b \\ c & -d-1 \end{pmatrix} \begin{pmatrix} x \\ y \end{pmatrix} + \begin{pmatrix} f(x,y) \\ g(x,y) \end{pmatrix} \tag{3.16}$$

in which f and g are higher order non-linear terms that we can substitute from our original model, expanded to cubic (system of Eqs. (3.6)):

$$f(x,y) = -ax(\frac{a^2x^2}{3} + b^2y^2) + by(\frac{b^2y^2}{3} + a^2x^2) \tag{3.17}$$

$$g(x,y) = -cx(\frac{c^2x^2}{3} + d^2y^2) + dy(\frac{d^2y^2}{3} + c^2x^2) \tag{3.18}$$

The coefficient matrix of the linearized system is called the *Jacobian matrix* and determines the type of the fixed point, its stability and the dynamics in its vicinity[8]. So the Jacobian matrix of the translated Wilson-Cowan model in Eq. (3.6) is:

$$J = \begin{pmatrix} a-1 & -b \\ c & -d-1 \end{pmatrix}. \tag{3.19}$$

To check the stability of the system and the type of bifurcation at the origin, we need to find the eigenvalues of the system:

$$\lambda_1 = \frac{1}{2}\left(-2 + a - d - \sqrt{a^2 - 4bc + 2ad + d^2}\right) \tag{3.20}$$

$$\lambda_2 = \frac{1}{2}\left(-2 + a - d + \sqrt{a^2 - 4bc + 2ad + d^2}\right) \tag{3.21}$$

We are interested in the Hopf bifurcation as we mentioned in the introduction. In order to have a Hopf bifurcation at the origin we should have pure imaginary

eigenvalues [8]. This constraint gives us two conditions for our bifurcation parameter, a (consequently α).

One constraint comes from the fact that to have pure imaginary eigenvalues, their real part should be zero, i.e. :

$$\frac{1}{2}(a-d-2)=0 \quad \Rightarrow \quad a=d+2 \tag{3.22}$$

The second constraint is that the discriminant should be negative to have an imaginary part for the eigenvalues, i.e. :

$$a^2-4bc+2ad+d^2<0 \tag{3.23}$$

By doing some algebra and make use of the first constraint Eq. (3.22), we get:

$$1-\sqrt{bc}<a<1+\sqrt{bc}\ . \tag{3.24}$$

As a consequent of Hopf bifurcation conditions above, it is easy to show that Eq. (3.24) reads the condition:

$$\alpha<|\omega| \tag{3.25}$$

$\alpha=0$ always satisfies this condition. Also at the bifurcation point, our Jacobian matrix Eq. (3.19) is anti-symmetric[28]. Hence $a=1$ or again $\alpha=0$ (which automatically yields to $d=-1$ from the Hopf bifurcation condition, Eq. (3.22)) and $b=c=\omega$. Then the system becomes:

$$\begin{pmatrix}\dot{x}\\ \dot{y}\end{pmatrix}=\begin{pmatrix}0 & -\omega\\ \omega & 0\end{pmatrix}\begin{pmatrix}x\\ y\end{pmatrix}+\begin{pmatrix}f(x,y)\\ g(x,y)\end{pmatrix}\ . \tag{3.26}$$

Now we can transform $x,y\longrightarrow z$ according to:

$$\begin{pmatrix}x\\ y\end{pmatrix}=\begin{pmatrix}1\\ -i\end{pmatrix}z+\begin{pmatrix}1\\ i\end{pmatrix}\bar{z} \tag{3.27}$$

which means: $x = z+\bar{z}$, $y = -iz+i\bar{z}$ and consequently: $\dot{x} = \dot{z}+\dot{\bar{z}}$ and $\dot{y} = -i\dot{z}+i\dot{\bar{z}}$. Now by substitution:

$$\begin{pmatrix} \dot{z}+\dot{\bar{z}} \\ -i\dot{z}+i\dot{\bar{z}} \end{pmatrix} = \begin{pmatrix} 0 & -\omega \\ \omega & 0 \end{pmatrix} \begin{pmatrix} z+\bar{z} \\ -iz+i\bar{z} \end{pmatrix} + \begin{pmatrix} f(z,\bar{z}) \\ g(z,\bar{z}) \end{pmatrix} \tag{3.28}$$

We can solve for $\dot{z}$ and obtain:

$$\dot{z} = i\omega z + \left(\frac{f+ig}{2}\right) \tag{3.29}$$

in which f and g are functions of z and $\bar{z}$ and can be obtained by applying the transformation of Eq. (3.27) to $f(x,y)$ and $g(x,y)$ in Eqs. (3.17) and (3.18):

$$f(z,\bar{z}) = -\frac{1}{3}\left((a+ib)z + (a-ib)\bar{z}\right)^3 \tag{3.30}$$

$$g(z,\bar{z}) = -\frac{1}{3}\left((c+id)z + (c-id)\bar{z}\right)^3 \tag{3.31}$$

These are the forms of f and g functions which should be used in Eq. (3.29). By this consideration we can rewrite Eq. (3.29) as below:

$$\dot{z} = i\omega z + q(z,\bar{z}) \tag{3.32}$$

where, $q(z,\bar{z}) = \left(\frac{f(z,\bar{z})+ig(z,\bar{z})}{2}\right)$.

By substituting functions f and g in q from Eqs. (3.30) and (3.31) we obtain the final format of Hopf normal form Eq. (3.15), at bifurcation point $\alpha = 0$.

The lines defined by $\dot{x} = 0$ and $\dot{y} = 0$ in any two dimensional system are called *nullclines*. We can compare the nullclines of translated Wilson-Cowan neural model with the ones obtained by the canonical model ($\dot{z} = 0$) as in Fig. (4). As one can see the nullclines coincide in the vicinity of origin (the fixed point), which is the point of interest.

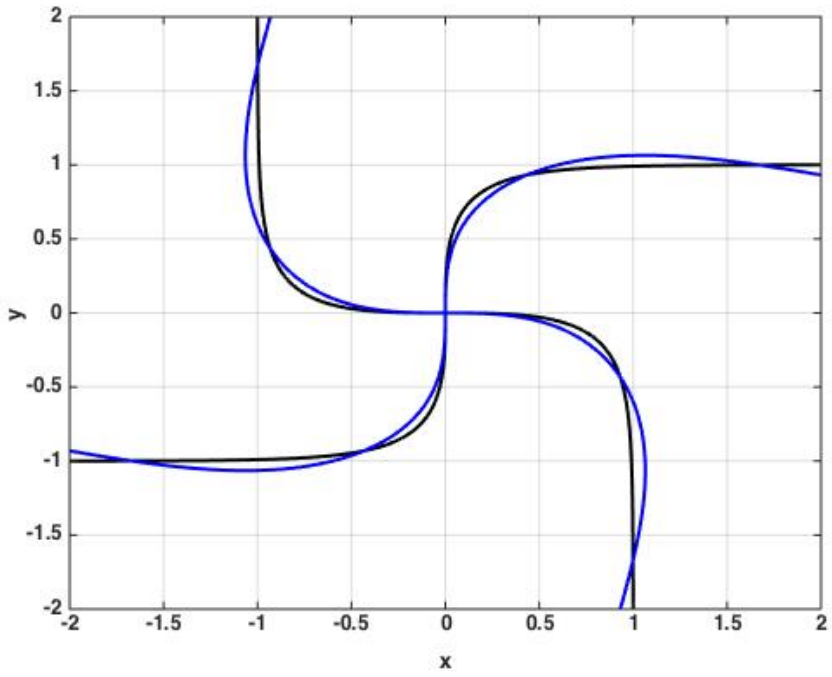

Figure 3.3: Nullclines of the both Wilson-Cowan (black) and Canonical (blue) model. Here $a = 1$, $b = c = \omega = 1.7$, $d = -1$, $\alpha = 0$, $\beta = -0.75$.

3.4 Deriving the canonical model for two coupled Wilson-Cowan oscillators

Now we consider two identical coupled Wilson-Cowan oscillators. As a physical example we can think of two neural populations that each oscillates intrinsically and they are connected to each other via synapses with some coupling strength. To analyze such system, we go back to our model (Eq. (3.2)) and replace for $i = j = 1, 2$. Since the two oscillators are identical, the feedback parameters are identical so we can write down synaptic and feedback parameters as follows:

$$a_{11} = a_{12} = a, b_{11} = b_{12} = b, c_{11} = c_{12} = c, d_{11} = d_{12} = d,$$

$$a_{12} = a_{21} = s_1, b_{12} = b_{21} = s_2, c_{12} = c_{21} = s_3, d_{12} = d_{21} = s_4$$

Also there is no external stimulus to the system, so $\rho_{x_1} = \rho_{x_2} = 0$. Considering these facts our model becomes:

$$\begin{cases} \dot{x_1} = -x_1 + S(ax_1 - by_1 + s_1x_2 - s_2y_2) \\ \dot{y_1} = -y_1 + S(cx_1 - dy_1 + s_3x_2 - s_4y_2) \\ \dot{x_2} = -x_2 + S(ax_1 - by_1 + s_1x_2 - s_2y_2) \\ \dot{y_2} = -y_2 + S(cx_1 - dy_1 + s_3x_2 - s_4y_2) \end{cases} \tag{3.33}$$

Also for small synaptic coefficients $s_1, .., s_4$, i.e. of the order $\epsilon \ll 1$ we can rescale the system as $s_k = \epsilon c_k$ for $k = 1, 2, 3, 4$. So we obtain the translated Wilson-Cowan model for two coupled identical oscillators by choosing tanh as our sigmoidal func-

tion which that after rescaling is described by[11]

$$\begin{cases} \dot{x_1} = -x_1 + \tanh(ax_1 - by_1) + \epsilon\ sech^2(ax_1 - by_1)(c_1x_2 - c_2y_2) \\ \dot{y_1} = -y_1 + \tanh(cx_1 - dy_1) + \epsilon\ sech^2(cx_1 - dy_1)(c_3x_2 - c_4y_2) \\ \\ \dot{x_2} = -x_2 + \tanh(ax_2 - by_2) + \epsilon\ sech^2(ax_2 - by_2)(c_1x_1 - c_2y_1) \\ \dot{y_2} = -y_2 + \tanh(cx_2 - dy_2) + \epsilon\ sech^2(cx_2 - dy_2)(c_3x_1 - c_4y_1) \end{cases} \tag{3.34}$$

3.4.1 The General Normal Form

As we did in section 3.3, we expand the trigonometric functions to cubic terms for both oscillators. Then, by going to the complex domain we can reduce the number of equations to two, instead of four:

$$\dot{s_i} = \dot{x_i} + i\dot{y_i} \tag{3.35}$$

If we expand this reduced system of equations, we figure out that some parts of the expansion represents exactly what we got for single oscillator and the other terms which all have the coupling coefficient ϵ forms the coupling therms. These are proven completely in Appendix..2. So we can rewrite Eqs. (3.35) as:

$$\dot{s_i} = \dot{s}_{is} + \ \epsilon\ \dot{s}_{ic} \tag{3.36}$$

By doing near identity change of variables:

$$s_i \longmapsto z_i + \kappa_i z_i^m \bar{z}_i^n \tag{3.37}$$

where m and n are positive integers that satisfy $m+n = 3$, like p and q, we obtain the final normal form of these two coupled oscillators:

$$\dot{z_i} = \dot{z}_{is} + \ \epsilon\ \dot{z}_{ic} \tag{3.38}$$

By doing some lengthy but straightforward algebra the results for $\dot{z}_{1_c}$ in Eqs. (3.38) can be written in 4 cases depending on the values of p, q, m and n which is completely presented in Appendix..2. The two cases for $\dot{z}_{1_s}$ has been already presented in section 3.3.1.

3.4.2 The Normal Form under Poincare-Andronov-Hopf Bifurcation Condition

As we argued in part 3.3.2 at the bifurcation point we must not have $m - n = -1$. So among all four cases in appendix .2 only the case for $m = 1$ and $n = 2$ is acceptable to represent Hopf bifurcation. Therefore the full canonical model that exhibits Hopf bifurcation for two coupled Wilson-Cowan oscillators up to quintic

terms is:

$$
\begin{cases}
\dot{z_1} = \dot{z_1}_s + \ \epsilon \ \dot{z_1}_c \\
\quad = A_1 z_1 + A_{21} z_1^2 \bar{z_1} \\
\quad\quad +\epsilon[B_1 z_2 + B_2 \bar{z_2} + B_5 z_1^2 z_2 + B_6 z_1^2 \bar{z_2} \\
\quad\quad +(B_7 - 2\kappa_1 \bar{B_2}) z_1 z_2 \bar{z_1} + (B_3 - B_1 \kappa_1) z_2 \bar{z_1}^2 \\
\quad\quad +(B_8 - 2\kappa_1 \bar{B_1}) z_1 \bar{z_1} \bar{z_2} + (B_4 - B_2 \kappa_1) \bar{z_1}^2 \bar{z_2} \\
\quad\quad +B_1 \kappa_2 z_2 \bar{z_2}^2 + B_2 \bar{\kappa_2} z_2^2 \bar{z_2}] \\
\dot{z_2} = \dot{z_2}_s + \ \epsilon \ \dot{z_2}_c \\
\quad = A_1 z_2 + A_{21} z_2^2 \bar{z_2} \\
\quad\quad +\epsilon[B_1 z_1 + B_2 \bar{z_1} + B_5 z_2^2 z_1 + B_6 z_2^2 \bar{z_1} \\
\quad\quad +(B_7 - 2\kappa_2 \bar{B_2}) z_1 z_2 \bar{z_2} + (B_3 - B_1 \kappa_2) z_1 \bar{z_2}^2 \\
\quad\quad +(B_8 - 2\kappa_2 \bar{B_1}) z_2 \bar{z_1} \bar{z_2} + (B_4 - B_2 \kappa_2) \bar{z_2}^2 \bar{z_1} \\
\quad\quad +B_1 \kappa_1 z_1 \bar{z_1}^2 + B_2 \bar{\kappa_1} z_1^2 \bar{z_1}]
\end{cases}
\tag{3.39}
$$

where all coefficients A_{21}, B and A_i, B_i for $i = 1, 2, ..., 8$ depends on synaptic and feedback parameters and have been calculated in appendices .1 and .2.

3.4.3 Radial and Angular solutions of each oscillator

One might be interested in calculating the phase and amplitude of oscillations for each oscillator in the coupled system (Eq. 3.38) under Hopf bifurcation. Starting off the normal form at Hopf bifurcation (Eqs. (3.39)), we can solve for the

amplitude and phase of each oscillator as below:

$$\dot{z_1} = A_1 z_1 + A_{21}|z_1|^2 z_1 + \epsilon \dot{z_{1c}} \tag{3.40}$$

$$\dot{z_2} = A_1 z_2 + A_{21}|z_2|^2 z_2 + \epsilon \dot{z_{2c}} \tag{3.41}$$

considering the polar transformation of $z_k : z_k = re^{i\phi_k}$, where the index k indicates each oscillator ($k = 1, 2$), represents this normal form in polar coordinates. We leave all the algebraic calculations in Appendix .3 and the final coupled nonlinear differential equations that governs the dynamics of the amplitudes and phases are:

$$\begin{aligned}
\dot{r_1} = {} & \alpha r_1 + \beta r_1^3 + \\
& \epsilon[n_1 \cos(\phi_2 - \phi_1) + n_2 \cos(\phi_2 + \phi_1)] r_2 \\
& + \epsilon[n_4 \cos(\phi_2 + \phi_1) \\
& + n_3 \cos(\phi_2 - \phi_1) + n_5 \cos(\phi_2 - 3\phi_1) + n_6 \cos(\phi_2 + 3\phi_1)] r_1^2 r_2 \\
& + \epsilon[n_7 \cos(\phi_1 + 3\phi_2) + n_8 \cos(\phi_2 + \phi_1)] r_2^3
\end{aligned} \tag{3.42}$$

$$\begin{aligned}
\dot{\phi_1} = {} & \omega + \delta r_1^2 \\
& + \epsilon[l_1 \sin(\phi_2 - \phi_1) + l_2 \sin(\phi_2 + \phi_1)] \frac{r_2}{r_1} \\
& + \epsilon[l_4 \sin(\phi_2 + \phi_1) \\
& + l_3 \sin(\phi_2 - \phi_1) + l_5 \sin(\phi_2 - 3\phi_1) + l_6 \sin(\phi_2 + 3\phi_1)] r_1 r_2 \\
& + \epsilon[l_7 \sin(\phi_1 + 3\phi_2) + l_8 \sin(\phi_2 + \phi_1)] \frac{r_2^3}{r_1}
\end{aligned} \tag{3.43}$$

where δ in the last two equations is the imaginary part of constant A_{21}. Note that the same form of equations can be obtained for the second oscillator by replacing index 1 by 2 for r and ϕ. We can derive a relationship for the relative phase between the two oscillators by defining $\phi(t) = \phi_1(t) - \phi_2(t)$ as the relative phase. For the

fixed point we have $\dot{r_1} = \dot{r_1} = 0$, which means amplitudes are time independent. Therefore the governing equation for relative phase is $\dot{\phi} = \dot{\phi_1} - \dot{\phi_2}$ and Eq. (3.43) can be used to replace for $\dot{\phi_1}$ and $\dot{\phi_2}$.

To show that $\phi^* = 0$ is a fixed point of the system, we demonstrate the solutions of $\dot{\phi}$ for different values of the bifurcation parameter α in Fig. (3.4).

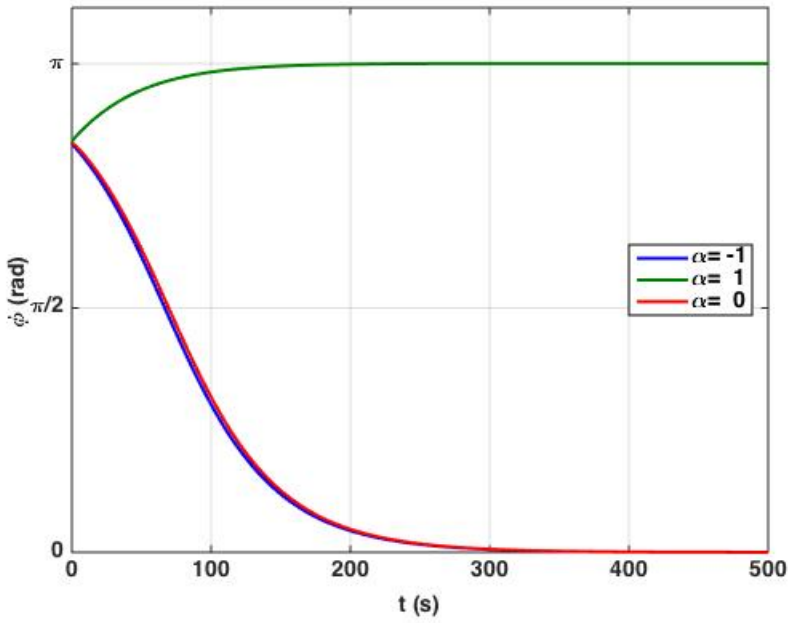

Figure 3.4: Solutions of the relative phase ϕ for different values of α. For the two cases of $\alpha < 0$ (damped) and $\alpha = 0$ (critical) the two oscillators become in phase with the relative phase of $\phi = 0$. Obviously the rate of change of ϕ for the damped oscillation is greater than the critical one. When $\alpha > 0$ (spontaneous), the two oscillators become anti-phase. In this figure $a = \alpha + 1$, $b = c = \omega = 10$, $d = a - 2$, $\epsilon = 0.1$, $c_1 = c_2 = c_3 = c_4 = \epsilon$, $\beta = A_{21}$ and $\delta = 0.1$. The initial conditions are $r_1 = r_2 = 1$, $\phi_1 = \pi$ and $\phi_2 = \pi/6$.

It might be useful pedagogically to note that the fixed points or equilibrium states of our system do not depend on the initial values of amplitude and phase.

In all initial conditions the relative phase converges to a fixed value. This is the beauty of dynamical systems theory where we do not need to solve our differential equations, necessarily.

3.5 The Average Relative Phase

In practice we are interested to find out the dynamics of the phase evolution of the two coupled oscillators described above. These oscillators as we mentioned might be coupled neurons in brain, or as another example two oscillating fingers or limbs under frequency scaling [8]. We look at

$$\dot{z_k} - A_1 z_k - A_{21}|z_k|^2 z_k = \epsilon \dot{z_k}(coupled), \tag{3.44}$$

which describes the dynamics of two coupled canonical oscillators where $k = 1, 2..$ we use the ansatz

$$z_k(t) = c_k(t)e^{i\omega_k t} + c_k^*(t)e^{-i\omega_k t} \tag{3.45}$$

as an approximate solution of this behaviour with $c_k(t) = r_k e^{i\phi_k(t)}$ as the time dependent amplitude of oscillations. ϕ_k and ω_k are the phase and frequency of the oscillations of each oscillator, respectively. We define the relative phase as $\phi(t) = \phi_1(t) - \phi_2(t)$, the difference between each oscillator's phase. Differentiating of this solution with respect to time leads to:

$$\dot{z_k}(t) = \dot{c_k}(t)e^{i\omega_k(t)} + \dot{c_k}^*(t)e^{-i\omega_k(t)} + i\omega_k c_k(t)e^{i\omega_k(t)} - i\omega_k {c_k}^*(t)e^{-i\omega_k(t)}. \tag{3.46}$$

Knowing that:

$$\dot{c_k}(t) = \dot{r}_k e^{i\phi_k(t)} + ir_k\dot{\phi}_k(t)e^{i\phi_k(t)} = (\dot{r}_k + ir_k\dot{\phi}_k(t))e^{i\phi_k(t)} \tag{3.47}$$

we can insert it in Eq. 3.46 to get:

$$\begin{aligned}\dot{z_k}(t) = (\dot{r}_k + ir_k\dot{\phi}_k(t))e^{i\phi_k(t)}e^{i\omega_k(t)} + (\dot{r}_k - ir_k\dot{\phi}_k(t))e^{-i\phi_k(t)}e^{-i\omega_k(t)} \\ + i\omega_k r_k e^{i\phi_k(t)}e^{i\omega_k(t)} - i\omega_k r_k e^{-i\phi_k(t)}e^{-i\omega_k(t)}.\end{aligned} \tag{3.48}$$

From now on we assume symmetric amplitude for both oscillators which means: $r_1 = r_2 = r$. Even if the amplitudes are asymmetric, the relative phase equation we will derive in the next pages, is still valid by assuming slowly varying amplitude approximation, i.e. $\dot{r}(t) \ll \omega$.

We write down the equations for the first oscillator . The left hand side of Eq. 3.44 is:

$$\begin{aligned}L.H.S = (\dot{r} + ir\dot{\phi_1})e^{i\phi_1}e^{i\omega_1(t)} + (\dot{r} - ir\dot{\phi_1})e^{-i\phi_1}e^{-i\omega_1(t)} \\ + i\omega_1 re^{i\phi_1}e^{i\omega_1(t)} - i\omega_1 re^{-i\phi_1}e^{-i\omega_1(t)} \\ - A_1[re^{i\phi_1}e^{i\omega_1(t)} + re^{-i\phi_1}e^{-i\omega_1(t)}] \\ - A_2[re^{-i\phi_1}e^{-i\omega_1(t)} + re^{i\phi_1}e^{i\omega_1(t)}] \\ A[re^{i\phi_1}e^{i\omega_1(t)} + re^{-i\phi_1}e^{-i\omega_1(t)}]^2[re^{-i\phi_1}e^{-i\omega_1(t)} + re^{i\phi_1}e^{i\omega_1(t)}]\end{aligned} \tag{3.49}$$

Multiply L.H.S by $e^{-i\phi_1}e^{-i\omega_1(t)}$:

$$\begin{aligned}L.H.S \times e^{-i\phi_1}e^{-i\omega_1(t)} = (\dot{r} + ir\dot{\phi_1}) + (\dot{r} - ir\dot{\phi_1})e^{-2i(\phi_1+\omega_1(t))} \\ + i\omega_1 r - i\omega_1 are^{-2i(\phi_1+\omega_1(t))} \\ - A_1[r + re^{-2i(\phi_1+\omega_1(t))}] - A_2[r + re^{-2i(\phi_1+\omega_1(t))}] \\ A[re^{i(\phi_1+\omega_1(t))} + re^{-i(\phi_1+\omega_1(t))}]^2[r + re^{-2i(\phi_1+\omega_1(t))}]\end{aligned} \tag{3.50}$$

Regrouping:

$$\begin{aligned} L.H.S \times e^{-i\phi_1} e^{-i\omega(t)} = \dot{r}(1 - e^{-2i(\phi_1+\omega(t))}) + \\ (ir\dot{\phi_1})(1 - e^{-2i(\phi_1+\omega(t))}) \\ + i\omega r(1 - e^{-2i(\phi_1+\omega(t))}) \\ - (A_1 + A_2)r(1 + e^{-2i(\phi_1+\omega(t))}) \\ - Ar^3(e^{i(\phi_1+\omega(t))} + e^{-i(\phi_1+\omega(t))})^2(1 + e^{-2i(\phi_1+\omega(t))}) \end{aligned} \tag{3.51}$$

It contains both oscillatory terms (exponential functions) with integer multiples of ω_1 as frequency and non-oscillating terms that do not contain these exponentials. By integrating over a period given by $T = \frac{2\pi}{\omega_1}$ all oscillatory terms vanish in such an average and only the non-oscillating terms survive. This process is called *averaging*:

$$L.H.S = \dot{r} + ir\dot{\phi_1} + i\omega_1 r - (A_1 + A_2)r \tag{3.52}$$

$$L.H.S = \dot{r} + ir(\dot{\phi_1} + \omega_1) - (A_1 + A_2)r \tag{3.53}$$

Substituting the solution on the right hand side (coupling term) of Eq. 3.44 and set $\epsilon = 1$ for now to ease the calculations:

$$\begin{aligned}
R.H.S = {} & B_1 r[e^{i(\phi_2+\omega_1(t))} + e^{-i(\phi_2+\omega_1(t))}] + B_2 r[e^{i(\phi_2+\omega_1(t))} + e^{-i(\phi_2+\omega_1(t))}] \\
& B_5 r^3[e^{i(\phi_1+\omega_1(t))} + e^{-i(\phi_1+\omega_1(t))}]^2[e^{i(\phi_2+\omega_1(t))} + e^{-i(\phi_2+\omega_1(t))}] \\
& B_6 r^3[e^{i(\phi_1+\omega_1(t))} + e^{-i(\phi_1+\omega_1(t))}]^2[e^{i(\phi_2+\omega_1(t))} + e^{-i(\phi_2+\omega_1(t))}] \\
& (B_7 - 2\kappa_1\bar{B_2}) r^3[e^{i(\phi_1+\omega_1(t))} + e^{-i(\phi_1+\omega_1(t))}]^2[e^{i(\phi_2+\omega_1(t))} + e^{-i(\phi_2+\omega_1(t))}] \\
& (B_3 - \kappa_1 B_1) r^3[e^{i(\phi_1+\omega_1(t))} + e^{-i(\phi_1+\omega_1(t))}]^2[e^{i(\phi_2+\omega_1(t))} + e^{-i(\phi_2+\omega_1(t))}] \\
& (B_8 - 2\kappa_1\bar{B_1}) r^3[e^{i(\phi_1+\omega_1(t))} + e^{-i(\phi_1+\omega_1(t))}]^2[e^{i(\phi_2+\omega_1(t))} + e^{-i(\phi_2+\omega_1(t))}] \\
& (B_4 - 2\kappa_1 B_2) r^3[e^{i(\phi_1+\omega_1(t))} + e^{-i(\phi_1+\omega_1(t))}]^2[e^{i(\phi_2+\omega_1(t))} + e^{-i(\phi_2+\omega_1(t))}] \\
& \kappa_2 B_1 r^3[e^{i(\phi_2+\omega_1(t))} + e^{-i(\phi_2+\omega_1(t))}]^3 \\
& \bar{\kappa_2} B_2 r^3[e^{i(\phi_2+\omega_1(t))} + e^{-i(\phi_2+\omega_1(t))}]^3
\end{aligned} \tag{3.54}$$

Recollecting the terms yield to:

$$\begin{aligned}
R.H.S. = {} & (B_1 + B_2) r[e^{i(\phi_2+\omega_1(t))} + e^{-i(\phi_2+\omega_1(t))}] \\
& + (B_3 + B_4 + B_5 + B_6 + B_7 + B_8 - \kappa_1(B_1 + B_2) - 2\kappa_1(\bar{B_1} + \bar{B_2})) \\
& [e^{i(\phi_1+\omega_1(t))} + e^{-i(\phi_1+\omega_1(t))}]^2[e^{i(\phi_2+\omega_1(t))} + e^{-i(\phi_2+\omega_1(t))}] \\
& + (B_1\kappa_2 + B_2\bar{\kappa_2}) r^3[e^{i(\phi_2+\omega_1(t))} + e^{-i(\phi_2+\omega_1(t))}]^3.
\end{aligned} \tag{3.55}$$

Introducing the new coefficients as:

$$\begin{cases}
M = B_1 + B_2 \\
N = B_3 + B_4 + B_5 + B_6 + B_7 + B_8 - \kappa_1 M - 2\kappa_1 \bar{M} \\
P = B_1\kappa_2 + B_2\bar{\kappa_2}
\end{cases} \tag{3.56}$$

gives a better representation:

$$\begin{aligned} R.H.S. = & Mr[e^{i(\phi_2+\omega_1(t))} + e^{-i(\phi_2+\omega_1(t))}] \\ & + Nr^2[e^{i(\phi_1+\omega_1(t))} + e^{-i(\phi_1+\omega_1(t))}]^2[e^{i(\phi_2+\omega_1(t))} + e^{-i(\phi_2+\omega_1(t))}] \\ & + Pr^3[e^{i(\phi_2+\omega_1(t))} + e^{-i(\phi_2+\omega_1(t))}]^3. \end{aligned} \tag{3.57}$$

Multiply the R.H.S. by $e^{-i(\phi_1+\omega_1 t)}$ gives:

$$\begin{aligned} R.H.S. = & Mr[e^{(i(\phi_2-\phi_1))} + e^{-i(\phi_2+\omega_1(t))}e^{-i(\phi_1+\omega_1(t))}] \\ & + Nr^3[e^{i(\phi_1+\omega_1(t))} + e^{-i(\phi_1+\omega_1(t))}]^2[e^{i(\phi_2-\phi_1)} + e^{-i(\phi_2+\phi_1+2\omega_1 t)}] \\ & + Pr^3[e^{i(\phi_2-\phi_1)} + e^{-i(\phi_2+\phi_1+2\omega_1 t)}]. \end{aligned} \tag{3.58}$$

By averaging only the first term survives and if we consider ϵ as before (not necessarily equal to 1):

$$R.H.S. = M\epsilon r e^{i(\phi_2-\phi_1)} = M\epsilon r e^{i\phi} \tag{3.59}$$

Now equating L.H.S. with R.H.S. and including the second oscillator by $1 \to 2$ and consequently $\phi \to -\phi$:

$$\begin{cases} \dot{r} + ir(\dot{\phi_1} + \omega_1) - (A_1 + A_2) = M\epsilon r e^{i\phi} \\ \dot{r} + ir(\dot{\phi_2} + \omega_2) - (A_1 + A_2) = M\epsilon r e^{-i\phi} \end{cases} \tag{3.60}$$

Subtracting second equation from the first one:

$$ir(\dot{\phi_1} - \dot{\phi_2} + \omega_1 - \omega_2) = M\epsilon r[e^{i\phi} - e^{-i\phi}], \tag{3.61}$$

by defining the relative frequency as $\omega = \omega_1 - \omega_2$ and using the relation $\sin\phi = \frac{e^{i\phi}-e^{-i\phi}}{2i}$:

$$-ir(\dot{\phi} - \omega) = M\epsilon r(2i\sin\phi). \tag{3.62}$$

Hence the average relative phase dynamics is given by:

$$\dot{\phi} = \omega - C \sin \phi. \tag{3.63}$$

where $C = 2M\epsilon$ is the total coupling coefficient and a complex number, due to M.

Let's replace for M the values of B_1 and B_2 (from equations) so that we find it in terms of the model parameters:

$$M = B_1 + B_2 = \frac{1}{2}[c_1 - c_4 + ic_2 + ic_3 + c_1 + c_4 + ic_3 - ic_2] = \frac{1}{2}[c_1 + 2ic_3] \tag{3.64}$$

hence:

$$M = c_1 + ic_3, \tag{3.65}$$

regardless of the values of c_2 and c_4. It means that the average phase dynamics of the system does not depend on the connection coefficients c_2 and c_4. Recall that M was introduced as one of the coupling coefficients and this also can be seen in the above equation which means M is a combination of the coupling coefficients of the basic model. This complex combination can be described as a phase difference between the rotation fo the two oscillators in phase space or a delay between their relative oscillations. By our definition, $C = 2M\epsilon$, so :

$$C = 2\epsilon(c_1 + ic_3). \tag{3.66}$$

Note that the magnitude of the total coupling coefficient is:

$$|C| = 2\epsilon\sqrt{c_1^2 + c_3^2}, \tag{3.67}$$

so it can be described as the coupling strength of the two oscillators.

Now we want to solve Eq. 3.63 for the relative phase ϕ. Rewriting Eq. 3.63:

$$\frac{d\phi}{dt} = \omega - C\sin\phi \tag{3.68}$$

so

$$dt = \frac{d\phi}{\omega - C\sin\phi} \tag{3.69}$$

and then we can integrate both sides to solve for t:

$$t = \int \frac{d\phi}{\omega - C\sin\phi} \tag{3.70}$$

By having the denominator equal to zero we can see that there is a pole at $\phi = \arcsin\frac{\omega}{C}$. This is indeed the steady-state solution of the relative phase. We will confirm this result as the steady-state in the next pages, by taking the limit of the solution as time tends to infinity. In the language of dynamical systems this is a fixed-point so:

$$\phi^* = \sin^{-1}\frac{\omega}{C}. \tag{3.71}$$

Eq. 3.71 shows that there should be a constraint in order to have a convergent answer and it is obvious that this constraint is:

$$-1 \leq \frac{\omega}{C} \leq 1 \tag{3.72}$$

therefore:

$$|\omega| \leq C. \tag{3.73}$$

This is the convergence interval in which we will evaluate the integral in Eq. 3.70. Before solving this integral we can take a look at the simpler case when the two

oscillators have the same frequency, consequently $\omega = 0$. So the integration process becomes simpler:

$$t = \int \frac{d\phi}{-C \sin\phi} \tag{3.74}$$

$$-Ct = \int \frac{d\phi}{\sin\phi} = \frac{1}{2} \ln(\tan\frac{\phi}{2}) + c \tag{3.75}$$

where c is the constant of integration and depends on the initial conditions. Solving this equation for ϕ:

$$\ln(\tan\frac{\phi}{2}) = -2(Ct + c) \Longrightarrow \tan\frac{\phi}{2} = \exp(-2(Ct + c)), \tag{3.76}$$

hence the relative phase is:

$$\phi = 2\tan^{-1}(e^{-2(Ct+c)}). \tag{3.77}$$

This result can be written in terms of the integration time interval, $\tau = c/C$:

$$\phi = 2\tan^{-1}(e^{-2C(t-\tau)}). \tag{3.78}$$

The plot of this relative phase is shown in the figure.4 below for some different initial conditions or better to say for a few different integration time intervals.

Going back to eq.3.70, we want to find the relative phase for the general case in which the frequency of the two oscillators is not the same necessarily, i.e. ω exists:

$$t = \int \frac{d\phi}{\omega - C \sin\phi}.$$

Within the convergence region ($|\omega| \leq C$) the answer of this integral is given by either:

$$t = -\frac{2}{\sqrt{C^2 - \omega^2}} \tanh^{-1}(\frac{\omega \tan\frac{\phi}{2} - C}{\sqrt{C^2 - \omega^2}}) + c \tag{3.79}$$

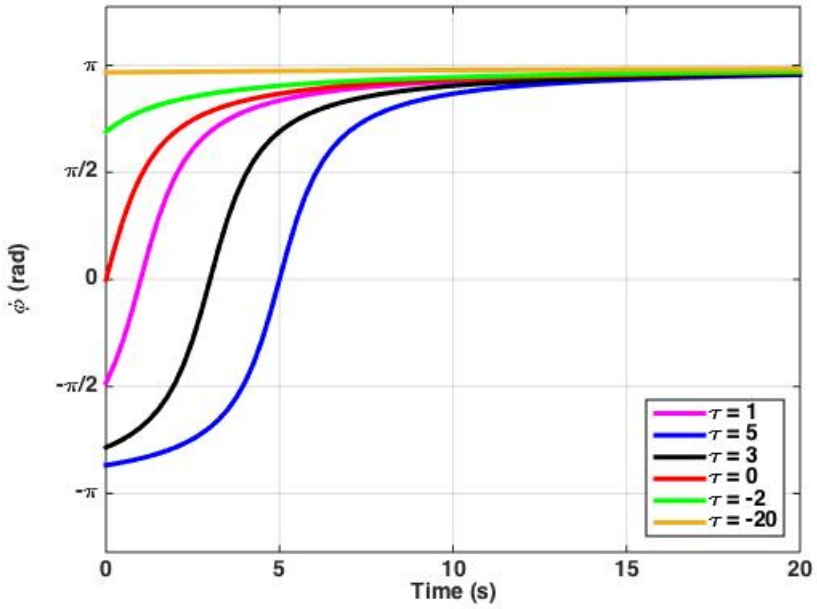

Figure 3.5: The relative phase (ϕ) as a function of time for different initial conditions While $C = 0.02$. This is a special case when the relative frequency of the oscillators is zero, which means they oscillate with the same frequency. One can see that they become phase-locked after sufficient time. In this special case, since $\omega = 0$ the fixed relative phase will be π .

or:

$$t = -\frac{2}{\sqrt{C^2 - \omega^2}} \coth^{-1}\left(\frac{\omega \tan\frac{\phi}{2} - C}{\sqrt{C^2 - \omega^2}}\right) + c \tag{3.80}$$

depending on the initial condition.

Hence the relative phase is given by:

$$\phi = 2\tan^{-1}\left\{\frac{\sqrt{C^2 - \omega^2}}{\omega} \tanh\left(\frac{-\sqrt{C^2 - \omega^2}(t - c)}{2}\right) + \frac{C}{\omega}\right\} \tag{3.81}$$

or:

$$\phi = 2\tan^{-1}\{\frac{\sqrt{C^2-\omega^2}}{\omega}\coth(\frac{-\sqrt{C^2-\omega^2}(t-c)}{2}) + \frac{C}{\omega}\}. \tag{3.82}$$

In either case if we take the limit of relative phase as time tends to infinity, we obtain the same result:

$$\lim_{t\to\infty}\phi = 2\tan^{-1}\{\frac{C-\sqrt{C^2-\omega^2}}{\omega}\}. \tag{3.83}$$

This angle should be the fixed-point or the steady-state solution that we have already mentioned, so we should indicate it with a star and:

$$\phi^* = 2\tan^{-1}\{\frac{C-\sqrt{C^2-\omega^2}}{\omega}\}. \tag{3.84}$$

But isn't it the same as the fixed-point we claimed in eq.3.71? Yes, and for the proof we need to recall:

$$\sin 2x = 2\sin x\cos x = 2\tan x\cos^2 x = \frac{2\tan x}{1+\tan^2 x}$$

so by considering x as $\frac{\phi^*}{2}$ we find:

$$\sin\phi^* = \frac{2(\frac{C-\sqrt{C^2-\omega^2}}{\omega})}{1+(\frac{C-\sqrt{C^2-\omega^2}}{\omega})^2} \tag{3.85}$$

and by expanding the denominator and a little algebra we will see that it is equal to: $\frac{\omega}{C}$, as we claimed in eq.3.71. In the figure below we illustrate some solutions of the relative phase for different initial conditions.

This convergence to a fixed-point is the *phase-locking* phenomenon. So after some time which is governed by the initial conditions of the two oscillators, they become *phase-locked*, i.e. they have a fixed phase difference which do not alter after a required time.

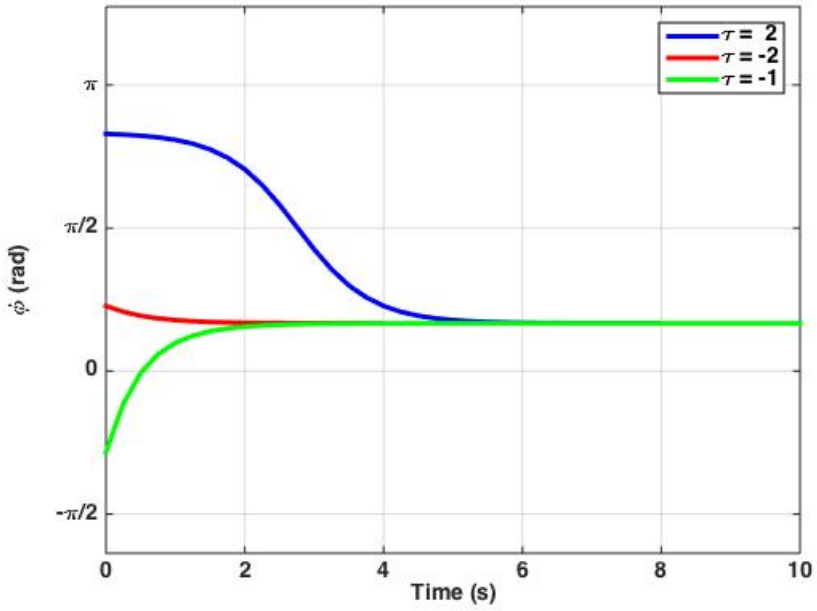

Figure 3.6: The relative phase (ϕ) as a function of time for different initial conditions while $C = 2$ and $\omega = 1$, so we can see the convergence of the solutions and *phase-locking* phenomenon. In this special case, since $\omega = 1$ and $C = 2$, the fixed relative phase will be $sin^{-1}(\frac{1}{2}) = \frac{\pi}{6}$.

3.6 Conclusion

We derived a canonical model out of Wilson-Cowan model for single and two coupled oscillators that represents all kinds of bifurcations depending on the nonlinear terms present in the Taylor expansion of the model. These Wilson-Cowan oscillators can be excitatory and inhibitory populations that are interconnected in different regions of the brain. Depending on the oscillatory regime and coupling strengths, these examples exhibit different types of bifurcations. This means the future of the system can be explained and predicted by knowing the type of phase

transition that will happen in the system. For example we have the development of periodic orbits (self-oscillations) from a stable fixed point (equilibrium), as a parameter (order parameter) crosses a critical value[28]. This type of phase transition refers to Hopf bifurcation. Calculating the Hopf bifurcation in the original Wilson-Cowan model is a difficult task. By obtaining the general normal form we found the bifurcation parameter of the system much easier for the case of Hopf bifurcation. We derived this special case in two different sections of the paper, one for a single oscillator and the other for coupled ones because of its importance in neuroscience . Stable oscillations in nonlinear waves may be another fruitful area and application[28]. We also obtained the time series diagrams for relative phase and amplitude of the two coupled oscillators. In this way we confirmed that the Hopf canonical model that we derived in the paper indeed exhibits Hopf bifurcation in the Wilson-Cowan model in a much easier way. By having the time series of the relative amplitude and phase of oscillators we can also obtain the period of oscillations and configure the equilibrium states of the systems. As a further step and application, if we know the anatomical properties of the nervous system in the brain which is unhealthy, by generalizing our model for population of neurons, we can treat the disease by changing the frequency of oscillations and consequently our order parameter α desirably. Good examples of these types of diseases are Tinnitus and Parkinson which are caused by unwanted oscillations of the nervous system.

Appendices

.1 Single oscillator analysis

Here is all calculations needed to continue after Eq. (3.10) to get the conventional normal form of Wilson-Cowan neural model Eq. (3.11).

In Eq. (3.10) we need to substitute for $\dot{s}$ from Eq. (3.7), but before doing that we try to make Eq. (3.7) simpler:

$$\dot{s} = A_1 s + A_2 \bar{s} + A_3 s^2 \bar{s} + A_4 s \bar{s}^2 + A_5 s^3 + A_6 \bar{s}^3. \tag{86}$$

Where the coefficients are:

$$\begin{cases} A_1 = \frac{1}{2}(-2 + a - d) + i\left(\frac{b+c}{2}\right) \\ A_2 = \frac{a+d}{2} + \frac{1}{2}i(-b + c) \\ A_3 = \frac{1}{8}\left(d^3 - a^3 - ab^2 + c^2 d\right) + \frac{1}{8}i\left(c^3 - a^2 b - b^3 - cd^2\right) \\ A_4 = -\frac{1}{8}\left(a^3 + ab^2 + c^2 d + d^3\right) + \frac{1}{8}i\left(c^3 + a^2 b + b^3 - cd^2\right) \\ A_5 = \frac{1}{24}\left(-a^3 + 3ab^2 + 3c^2 d - d^3\right) + \frac{1}{24}i\left(-3a^2 b + b^3 + c^3 + 3cd^2\right) \\ A_6 = \frac{1}{24}\left(-a^3 + 3ab^2 - 3c^2 d + d^3\right) + \frac{1}{24}i\left(3a^2 b - b^3 + 3cd^2 + c^3\right). \end{cases} \tag{87}$$

with this substitution for $\dot{s}$, Eq. (3.10) becomes:

$$\begin{aligned}\dot{z} &= A_1 s + A_2 \bar{s} + A_3 s^2 \bar{s} + A_4 s \bar{s}^2 + A_5 s^3 + A_6 \bar{s}^3 \\ &\quad - \kappa p s^{p-1} \bar{s}^q \left(A_1 s + A_1 \bar{s}\right) - \kappa q s^p \bar{s}^{q-1} \left(\bar{A}_1 \bar{s} + \bar{A}_1 s\right) \ .\end{aligned} \tag{88}$$

we omit *h.o.t.* in our calculations from now on, since we are dealing with cubic terms and lower.

Now we transform all s and $\bar{s}$ on the right hand side of equation 88 according to the near identity change of variable in Eq. (3.8) to get the final normal form:

$$\begin{aligned}\dot{z} &= A_1 z + A_2 \bar{z} + A_3 z^2 \bar{z} + A_4 z \bar{z}^2 + A_5 z^3 + A_6 \bar{z}^3 \\ &\quad + A_1 \kappa z^p \bar{z}^q + A_2 \bar{\kappa} z^q \bar{z}^p \\ &\quad - \bar{A}_2 q \kappa z^{p+1} \bar{z}^{-1+q} - \bar{A}_1 q \kappa z^p \bar{z}^q - A_1 p \kappa z^p \bar{z}^q - A_2 p \kappa z^{-1+p} \bar{z}^{q+1}\end{aligned} \tag{89}$$

Eq. (89) is the general version of the conventional normal form (CNF). By choosing p and q such that their addition is the order of the monomials that we want to remove, we can eliminate many of the monomials and get simpler formats. Since here we are interested in removing monomials with orders higher than cubic $p + q = 3$ and there will be two choices for p and q, either $p = 1, q = 2$ or $p = 2, q = 1$. Note that we have made the transformation as $z \longmapsto z + h(z, \bar{z})$ for some $h = z^p \bar{z}^q$, where $p + q$ is the order of the term that we want to simplify and $p, q \in \aleph$. So we consider these two cases as $case(i)$ and $case(ii)$.

- $case(i) : p = 1, q = 2$

  In Eq. (89), if we set $p = 1$ and $q = 2$, after collecting the terms we will get:

$$\begin{aligned}\dot{z} &= A_1 z + A_2 \bar{z} + \left(A_4 - 2\kappa \bar{A}_1\right) z \bar{z}^2 + \left(A_3 - 2\kappa \bar{A}_2 + A_2 \bar{\kappa}\right) z^2 \bar{z} \\ &\quad + A_5 z^3 + (A_6 - A_2 \kappa) \bar{z}^3\end{aligned} \tag{90}$$

Using the fact that $z\bar{z} = |z|^2$ and applying normal form method successively to eliminate terms that contain z^3 and $\bar{z}^3$ we obtain:

$$\begin{aligned} \dot{z} &= A_1 z + A_2 \bar{z} \\ &+ \left(A_4 - 2\kappa \bar{A}_1\right) |z|^2 \bar{z} + \left(A_3 - 2\kappa \bar{A}_2 + A_2 \bar{\kappa}\right) z |z|^2 \end{aligned} \tag{91}$$

If we set $\kappa = \dfrac{A_4}{2\bar{A}_1}$ we can remove one more term which is $|z|^2\bar{z}$. Then the Normal Form becomes:

$$\dot{z} = A_1 z + A_2 \bar{z} + \left(A_3 - 2\kappa \bar{A}_2 + A_2 \bar{\kappa}\right) z|z|^2 \tag{92}$$

Introducing A_{21} so that $A_{21} = A_3 - 2\kappa\bar{A}_2 + A_2\bar{\kappa}$, yields the normal form when $p = 1$ and $q = 2$:

$$\dot{z} = A_1 z + A_2 \bar{z} + A_{21} z|z|^2 \tag{93}$$

- *case(ii)* : $p = 2, q = 1$

  In a similar fashion, but this time with $p = 2$ and $q = 1$ we can eliminate other terms. Again by starting off from equation 89 and collecting the terms we get:

$$\begin{aligned} \dot{z} &= A_1 z + A_2 \bar{z} + \left(A_4 - 2A_2\kappa + A_2\bar{\kappa}\right) z\bar{z}^2 + \left(A_3 - A_1\kappa - \kappa\bar{A}_1\right) z^2\bar{z} \\ &+ \left(A_5 - \kappa\bar{A}_2\right) z^3 + A_6\bar{z}^3 \end{aligned} \tag{94}$$

  Using the fact that $z\bar{z} = |z|^2$ and applying normal form method successively to eliminate terms that contain z^3 and $\bar{z}^3$ we get:

$$\begin{aligned} \dot{z} &= A_1 z + A_2 \bar{z} \\ &+ \left(A_4 - 2A_2\kappa + A_2\bar{\kappa}\right) |z|^2 \bar{z} + \left(A_3 - A_1\kappa - \kappa\bar{A}_1\right) z |z|^2 \end{aligned} \tag{95}$$

Let's choose $\kappa = \dfrac{A_3}{A_1 + \bar{A}_1}$ such that the last term on the right hand side cancels out. By introducing $A_{12} = A_4 - 2A_2\kappa + A_2\bar{\kappa}$ we end up with the final normal form for this particular case:

$$\dot{z} = A_1 z + A_2 \bar{z} + A_{12}|z|^2 \bar{z} \tag{96}$$

In summary:

- $case(i) \ : p = 1, q = 2 \Rightarrow \dot{z}_s = A_1 z + A_2 \bar{z} + A_{21}|z|^2 z$
- $case(ii) : p = 2, q = 1 \Rightarrow \dot{z}_s = A_1 z + A_2 \bar{z} + A_{12}|z|^2 \bar{z}$

we replace $\dot{z}$ by $\dot{z}_s$ to show that this normal form is for a single oscillator.

.2 coupled oscillators analysis

Now we replace the full expansion of the Cartesian components for each oscillator from the Eqs. (3.34), but for time saving and easy writing we just do the calculations for the first oscillator, since the equations are the same for the second oscillator and can be obtained by replacing the indices: $1 \to 2$.

$$\begin{aligned}
\dot{s_1} = \dot{x_1} + i\dot{y_1} \\
&= (a-1)x_1 - by_1 - ax_1(\frac{a^2x_1^2}{3} + b^2y_1^2) + by_1(\frac{b^2y_1^2}{3} + a^2x_1^2) \\
&+ \epsilon(c_1x_2 - c_2y_2)(1 + 2abx_1y_1 - a^2x_1^2 - b^2y_1^2) \\
&+ i[-(d+1)y_1 + cx_1 + dy_1(\frac{d^2y_1^2}{3} + c^2x_1^2) - cx_1(\frac{c^2x_1^2}{3} + d^2y_1^2) \\
&+ \epsilon(c_3x_2 - c_4y_2)(1 + 2cdx_1y_1 - c^2x_1^2 - d^2y_1^2)]
\end{aligned} \tag{97}$$

by recollecting the terms we can separate the right hand side to two main sentences, the first sentence is for the uncoupled oscillation and the second one with ϵ as coefficient describes the coupling:

$$\begin{aligned}
\dot{s_1} &= \dot{x_1} + i\dot{y_1} \\
&= [(a-1+ic)x_1 - (b+i(d+1))y_1 \\
&- (ab^2+icd^2)x_1y_1^2 + (a^2b+ic^2d)x_1^2y_1 - (\frac{a^3+ic^3}{3})x_1^3 + (\frac{b^3+id^3}{3})y_1^3] \\
&+ \epsilon[(c_1+ic_3)x_2 - (c_2+ic_4)y_2 \\
&\quad + x_1y_1(2abc_1+2icdc_3)x_2 - x_1y_1(2abc_2+2icdc_4)y_2 \\
&\quad - y_1^2(c_1b^2+ic_3d^2)x_2 + y_1^2(c_2b^2+ic_4d^2)y_2 \\
&\quad - x_1^2(c_1a^2+ic_3c^2)x_2 + x_1^2(c_2a^2+ic_4c^2)y_2] \\
&= \dot{s_{1s}} + \epsilon\dot{s_{1c}}
\end{aligned} \tag{98}$$

the first bracket is what we already got for single oscillator in section 3.3 and the second bracket is because of the coupling. The index "s" refers to the terms for a single oscillator and the index "c" refers to coupling terms. Let's just work out $\dot{s_{1c}}$, since we have already done the first part($\dot{s_{1s}}$):

$$\begin{aligned}
\dot{s_{1c}} = &\\
&(c_1+ic_3)x_2 - (c_2+ic_4)y_2 \\
&+ x_1y_1(2abc_1+2icdc_3)x_2 - x_1y_1(2abc_2+2icdc_4)y_2 \\
&- y_1^2(c_1b^2+ic_3d^2)x_2 + y_1^2(c_2b^2+ic_4d^2)y_2 \\
&- x_1^2(c_1a^2+ic_3c^2)x_2 + x_1^2(c_2a^2+ic_4c^2)y_2
\end{aligned} \tag{99}$$

since $x_i = \frac{s_i+\bar{s_i}}{2}$ and $y_i = \frac{s_i-\bar{s_i}}{2}$ with $i = 1, 2$ we can replace for x_i and y_i in above equations so we get the right hand side in terms of s and $\bar{s}$:

$$\begin{aligned} \dot{s_{1c}} = \\ & B_1 s_2 + B_2 \bar{s_2} + B_3 \bar{s_1}^2 s_2 + B_4 \bar{s_1}^2 \bar{s_2} \\ & B_5 s_1^2 s_2 + B_6 \bar{s_2} + B_7 s_1 \bar{s_1} s_2 + B_8 s_1 \bar{s_1} \bar{s_2} \end{aligned} \tag{100}$$

where:

$$\begin{cases} B_1 = \frac{1}{2}(c_1 - c_4 + i(c_2 + c_3)) \\ B_2 = \frac{1}{2}(c_1 + c_4 + i(c_3 - c_2)) \\ B_3 = \frac{1}{8}((c - id)^2(c_4 - ic_3) - ic_2(a - ib)^2 - c_1(a - ib)^2) \\ B_4 = \frac{1}{8}(-c_1(a - ib)^2 + i(c_2(a - ib)^2 - (c - id)^2(c_3 - ic_4))) \\ B_5 = \frac{1}{8}(-c_1(a - ib)^2 - ic_2(a + ib)^2 - (c + id)^2(c_4 - ic_3)) \\ B_6 = \frac{1}{8}(-c_1(a + ib)^2 + i(c_2(a + ib)^2 - (c + id)^2(c_3 - ic_4))) \\ B_7 = \frac{1}{4}(-c_1(a^2 + b^2) - i(c_2(a^2 + b^2) + (c^2 + d^2)(c_3 + ic_4))) \\ B_8 = \frac{1}{4}(-c_1(a^2 + b^2) + i(c_2(a^2 + b^2) - (c^2 + d^2)(c_3 - ic_4))) \end{cases} \tag{101}$$

where p, q, m and n are positive integers. Now is the time for near identity change of variable:

$$\begin{cases} s_1 \longmapsto z_1 + \kappa_1 z_1^p \bar{z_1}^q \\ s_2 \longmapsto z_2 + \kappa_2 z_2^m \bar{z_2}^n \end{cases} \tag{102}$$

The procedure is the same as what we did in part 3.3.1 for single oscillator. Rewriting the transformation gives us: $z_1 = s_1 - \kappa_1 z_1^p \bar{z_1}^q$ and $z_2 = s_2 \kappa_2 z_2^m \bar{z_2}^n$ and:

$$z_{1c} = s_1 - \kappa_1 s_1^p \bar{s_1}^q \tag{103}$$

and the same format for the second oscillator with replacing 1 by 2 and (p, q) with (m, n). Continuing with the first oscillator and differentiating Eq. (103) :

$$\dot{z_{1c}} = \dot{s_{1c}} - p\kappa_1 s_1^{p-1}\dot{s_{1c}}\bar{s_1}^q - \kappa_1 q s_1^p \bar{s_1}^{q-1}\dot{\bar{s}_{1c}} \tag{104}$$

in this equation we will substitute for $\dot{s_1}$ from Eq. (100) completely but for the second and third term on the right hand side we don't need it completely and we just replace the linear parts of Eq. (100) since the rest are the terms with more than cubic order. Hence we'll get:

$$\begin{aligned}\dot{z_{1c}} = \\ & B_1 s_2 + B_2\bar{s_2} + B_3\bar{s_1}^2 s_2 + B_4\bar{s_1}^2\bar{s_2} \\ & B_5 s_1^2 s_2 + B_6 s_1^2\bar{s_2} + B_7 s_1\bar{s_1}s_2 + B_8 s_1\bar{s_1}\bar{s_2} \\ & - p\kappa_1 s_1^{p-1}\bar{s_1}^q(B_1 s_2 + B_2\bar{s_2}) - \kappa_1 q s_1^p\bar{s_1}^{q-1}(\bar{B_1}\bar{s_2} + \bar{B_2}s_2)\end{aligned} \tag{105}$$

Back to the original transformation (Eq. (102)) and eliminating all terms with order more than cubic ($p+q = m+n = 3$) we will obtain the normal form for the coupled part of the oscillations:

$$\begin{aligned}\dot{z_{1c}} = \\ & B_1 z_2 + B_5 z_1^2 z_2 + B_7 z_1 z_2 \bar{z1} + B_3 z_2\bar{z_1}^2 + B_2\bar{z_2} + B_6 z_1^2\bar{z_2} \\ & + B_8 z_1\bar{z_1}\bar{z_2} + B_4\bar{z_1}^2\bar{z_2} + B_1 z_2^m\kappa_2\bar{z_2}^n - q\kappa_1\bar{B_2}z_1^p\bar{z_1}^{q-1}z_2 \\ & - q\kappa_1\bar{B_1}z_1^p\bar{z_2}\bar{z_1}^{q-1} - B_1 p\kappa_1 z_1^{p-1}\bar{z1}^q z_2 \\ & - B_2 p\kappa_1 z_1^{p-1}\bar{z_1}^q\bar{z2} + B_2 z_2^n\bar{z_2}^m\bar{\kappa_2}\end{aligned} \tag{106}$$

Therefore we have four cases depending on the value of p, q, m and n.They will be obtained by choosing the value of 1 and 2 for these parameters successively. The results for the normal form are:

- $case(i)\ :\ p=1,q=2\ ;\ m=1,n=2$

  $\dot{z}_{1c} = B_1 z_2 + B_2 \bar{z_2} + B_5 z_1^2 z_2 + B_6 z_1^2 \bar{z_2}$

  $(B_7 - 2\kappa_1 \bar{B_2}) z_1 z_2 \bar{z_1} + (B_3 - B_1 \kappa_1) z_2 \bar{z_1}^2$

  $(B_8 - 2\kappa_1 \bar{B_1}) z_1 \bar{z_1} \bar{z_2} + (B_4 - B_2 \kappa_1) \bar{z_1}^2 \bar{z_2}$

  $B_1 z_2 \kappa_2 \bar{z_2}^2 + B_2 \bar{\kappa_2} z_2^2 \bar{z_2}$

- $case(ii)\ :\ p=2,q=1\ ;\ m=1,n=2$

  $\dot{z}_{1c} = B_1 z_2 + b_2 \bar{z_2} + B_3 z_2 \bar{z_1}^2 + B_4 \bar{z_1}^2 \bar{z_2}$

  $(B_5 - \kappa_1 \bar{B_2}) z_1^2 z_2 + (B_6 - \kappa_1 \bar{B_1}) z_1^2 \bar{z_2}$

  $(B_7 - 2\kappa_1 \bar{B_1}) z_1 z_2 \bar{z_1} + (B_8 - 2\kappa_1 B_2) z_1 \bar{z_1} \bar{z_2}$

  $B_1 z_2 \kappa_2 \bar{z_2}^2 + B_2 \bar{\kappa_2} z_2^2 \bar{z_2}$

- $case(iii)\ :\ p=1,q=2\ ;\ m=2,n=1$

  $\dot{z}_{1c} = B_1 z_2 + B_5 z_1^2 z_2 + B_2 \bar{z_1} + B_6 z_1^2 \bar{z_2}$

  $+(B_3 - B_1 \kappa_1) z_2 \bar{z_1}^2 + (B_4 - B_2 \kappa_1) \bar{z_2} \bar{z_1}^2$

  $+(B_7 - 2\bar{B_2} \kappa_1) z_1 z_2 \bar{z_1} + (B_8 - 2\bar{B_1} \kappa_1) z_1 \bar{z_1} \bar{z_2}$

  $+B_1 \kappa_2 z_2^2 \bar{z_2} + B_2 \bar{\kappa_2} z_2 \bar{z_2}^2$

- $case(iv)\ :\ p=2,q=1\ ;\ m=2,n=1$

  $\dot{z}_{1c} = B_1 z_2 + B_3 \bar{z_1}^2 z_2 + B_2 \bar{z_2} + B_4 \bar{z_1}^2 \bar{z_2}$

  $+(B_5 - \bar{B_2} \kappa_1) z_2 z_1^2 + (B_6 - \bar{B_1} \kappa_1) \bar{z_2} z_1^2$

  $+(B_7 - 2B_1 \kappa_1) z_1 z_2 \bar{z_1} + (B_8 - 2B_2 \kappa_1) z_1 \bar{z_1} \bar{z_2}$

  $+B_1 \kappa_2 z_2^2 \bar{z_2} + B_2 \bar{\kappa_2} z_2 \bar{z_2}^2$

.3 radial and angular equations

Starting off the normal form at Hopf bifurcation (Eqs. (3.39)), we can solve for the amplitude and phase of each oscillator as below:

$$\dot{z_1} = A_1 z_1 + A_{21}|z_1|^2 z_1 + \epsilon \dot{z_{1c}} \tag{107}$$

$$\dot{z_2} = A_1 z_2 + A_{21}|z_2|^2 z_2 + \epsilon \dot{z_{2c}} \tag{108}$$

considering the polar transformation of z_k : $z_k = re^{i\phi_k}$, where the index k indicates each oscillator ($k = 1, 2$), represents this normal form in polar coordinates.

$$e^{i\phi_1}(\dot{r_1} + ir_1\dot{\phi_1}) = A_1 r_1 e^{i\phi_1} + Ar_1^3 e^{i\phi_1} + \epsilon \dot{z_{1c}} \tag{109}$$

$$e^{i\phi_2}(\dot{r_2} + ir_2\dot{\phi_2}) = A_1 r_2 e^{i\phi_2} + Ar_2^3 e^{i\phi_2} + \epsilon \dot{z_{2c}} \tag{110}$$

we left the transformation for the coupling term, but we will get back to it soon. The above equations can be written as below by dividing both sides by $e^{i\phi_k}$:

$$\dot{r_1} + ir_1\dot{\phi_1} = A_1 r_1 + Ar_1^3 + \epsilon \dot{z_{1c}} e^{-i\phi_1} \tag{111}$$

$$\dot{r_2} + ir_2\dot{\phi_2} = A_1 r_2 + Ar_2^3 + \epsilon \dot{z_{2c}} e^{-i\phi_2} \tag{112}$$

The real and imaginary parts of these equations provide us with the amplitude and phase of each oscillator, respectively:

$$\dot{r_1} = Re(A_1)r_1 + Re(A)r_1^3 + \epsilon Re(\dot{z_{1c}} e^{-i\phi_1}) \tag{113}$$

$$\dot{r_2} = Re(A_1)r_2 + Re(A)r_2^3 + \epsilon Re(\dot{z_{2c}} e^{-i\phi_2}) \tag{114}$$

$$\dot{\phi_1} = Im(A_1) + Im(A)r_1^2 + \frac{\epsilon}{r_1} Im(\dot{z_{1c}} e^{-i\phi_1}) \tag{115}$$

$$\dot{\phi_2} = Im(A_1) + Im(A)r_2^2 + \frac{\epsilon}{r_2} Im(\dot{z_{2c}} e^{-i\phi_2}) \tag{116}$$

Now we need to substitute for $\dot{z_{kc}}$ from $case(i)$ and separate real and imaginary parts to continue the calculations for amplitude and phase of each oscillator, respectively. We leave all the algebraic calculations in appendix .3.

$$\begin{aligned}
\dot{z_{1c}}e^{-i\phi_1} = & B_1 r_2 e^{i(\phi_2-\phi_1)} \\
& + [B_2 r_2 + B_1\kappa_2 r_2^3]e^{-i(\phi_2+\phi_1)} \\
& + [B_5 + B_7 - 2\kappa_1\bar{B_2}]r_1^2 r_2 e^{i(\phi_2+\phi_1)} \\
& + [B_8 + B_6 - 2\kappa_1\bar{B_1}]r_1^2 r_2 e^{-i(\phi_2-\phi_1)} \\
& + [B_3 - \kappa_1 B_1]r_1^2 r_2 e^{i(\phi_2-3\phi_1)} \\
& + [B_4 - \kappa_1 B_2]r_1^2 r_2 e^{-i(\phi_2+3\phi_1)} \\
& + [\bar{\kappa_2} B_2]r_2^3 e^{-i(\phi_1+3\phi_2)}
\end{aligned} \tag{117}$$

real and imaginary parts:

$$\begin{aligned}
Re(\dot{z_{1c}}e^{-i\phi_1}) = & Re(B_1) r_2 \cos(\phi_2-\phi_1) \\
& + Re[B_2 r_2 + B_1\kappa_2 r_2^3]\cos(\phi_2+\phi_1) \\
& + Re[B_5 + B_7 - 2\kappa_1\bar{B_2}]r_1^2 r_2 \cos(\phi_2+\phi_1) \\
& + Re[B_8 + B_6 - 2\kappa_1\bar{B_1}]r_1^2 r_2 \cos(\phi_2-\phi_1) \\
& + Re[B_3 - \kappa_1 B_1]r_1^2 r_2 \cos(\phi_2-3\phi_1) \\
& + Re[B_4 - \kappa_1 B_2]r_1^2 r_2 \cos(\phi_2+3\phi_1) \\
& + Re[\bar{\kappa_2} B_2]r_2^3 \cos(\phi_1+3\phi_2)
\end{aligned} \tag{118}$$

$$
\begin{aligned}
Im(\dot{z_{1c}}e^{-i\phi_1}) = {} & Im(B_1)r_2\sin(\phi_2-\phi_1) \\
& + Im[B_2r_2 + B_1\kappa_2 r_2^3]\sin(\phi_2+\phi_1) \\
& + Im[B_5 + B_7 - 2\kappa_1\bar{B_2}]r_1^2 r_2\sin(\phi_2+\phi_1) \\
& + Im[B_8 + B_6 - 2\kappa_1\bar{B_1}]r_1^2 r_2\sin(\phi_2-\phi_1) \\
& + Im[B_3 - \kappa_1 B_1]r_1^2 r_2\sin(\phi_2-3\phi_1) \\
& + Im[B_4 - \kappa_1 B_2]r_1^2 r_2\sin(\phi_2+3\phi_1) \\
& + Im[\bar{\kappa_2}B_2]r_2^3\sin(\phi_1+3\phi_2)
\end{aligned}
\tag{119}
$$

Recollecting:

$$
\begin{aligned}
Re(\dot{z_{1c}}e^{-i\phi_1}) = {} & r_2[n_1\cos(\phi_2-\phi_1) + n_2\cos(\phi_2+\phi_1)] \\
& + r_1^2 r_2[n_4\cos(\phi_2+\phi_1) \\
& + n_3\cos(\phi_2-\phi_1) + n_5\cos(\phi_2-3\phi_1) + n_6\cos(\phi_2+3\phi_1)] \\
& + r_2^3[n_7\cos(\phi_1+3\phi_2) + n_8\cos(\phi_2+\phi_1)]
\end{aligned}
\tag{120}
$$

$$
\begin{aligned}
\frac{Im(\dot{z_{1c}}e^{-i\phi_1})}{r_1} = {} & \frac{r_2}{r_1}[l_1\sin(\phi_2-\phi_1) + l_2\sin(\phi_2+\phi_1)] \\
& + r_1 r_2[l_4\sin(\phi_2+\phi_1) \\
& + l_3\sin(\phi_2-\phi_1) + l_5\sin(\phi_2-3\phi_1) + l_6\sin(\phi_2+3\phi_1)] \\
& + \frac{r_2^3}{r_1}[l_7\sin(\phi_1+3\phi_2) + l_8\sin(\phi_2+\phi_1)]
\end{aligned}
\tag{121}
$$

where:

$$
n_1 = Re(B_1), n_2 = Re(B_2), n_3 = Re(B_8 + B_6 - 2\kappa_1\bar{B_1}), n_4 = Re(B_5 + B_7 - 2\kappa_1\bar{B_2})
$$

$$
n_5 = Re(B_3 - \kappa_1 B_1), n_6 = Re(B_4 - \kappa_1 B_2), n_7 = Re(\bar{\kappa_2}B_2), n_8 = Re(\kappa_2 B_1)
$$

and:

$$l_1 = Im(B_1), l_2 = Im(B_2), l_3 = Im(B_8 + B_6 - 2\kappa_1\bar{B_1}), l_4 = Im(B_5 + B_7 - 2\kappa_1\bar{B_2})$$

$$l_5 = Im(B_3 - \kappa_1 B_1), l_6 = Im(B_4 - \kappa_1 B_2), l_7 = Im(\bar{\kappa_2} B_2), l_8 = Im(\kappa_2 B_1).$$

Therefore the radial and angular equations for each oscillator becomes(The choice of n and l as coefficients goes back to radial and angular numbers in Quantum Mechanics.):

$$\begin{aligned}
\dot{r_1} = & Re(A_1)r_1 + Re(A)r_1^3 + \\
& \epsilon\{r_2[n_1\cos(\phi_2 - \phi_1) + n_2\cos(\phi_2 + \phi_1)] \\
& + r_1^2 r_2[n_4\cos(\phi_2 + \phi_1) \\
& + n_3\cos(\phi_2 - \phi_1) + n_5\cos(\phi_2 - 3\phi_1) + n_6\cos(\phi_2 + 3\phi_1)] \\
& + r_2^3[n_7\cos(\phi_1 + 3\phi_2) + n_8\cos(\phi_2 + \phi_1)]\}
\end{aligned} \tag{122}$$

$$\begin{aligned}
\dot{r_2} = & Re(A_1)r_2 + Re(A)r_2^3 + \\
& \epsilon\{r_1[n_1\cos(\phi_2 - \phi_1) + n_2\cos(\phi_2 + \phi_1)] \\
& + r_2^2 r_1[n_4\cos(\phi_2 + \phi_1) \\
& + n_3\cos(\phi_2 - \phi_1) + n_5\cos(\phi_1 - 3\phi_2) + n_6\cos(\phi_1 + 3\phi_2)] \\
& + r_1^3[n_7\cos(\phi_2 + 3\phi_1) + n_8\cos(\phi_2 + \phi_1)]\}
\end{aligned} \tag{123}$$

$$\begin{aligned}
\dot{\phi_1} = & Im(A_1) + Im(A)r_1^2 \\
& + \epsilon\{\frac{r_2}{r_1}[l_1\sin(\phi_2 - \phi_1) + l_2\sin(\phi_2 + \phi_1)] \\
& + r_1 r_2[l_4\sin(\phi_2 + \phi_1) \\
& + l_3\sin(\phi_2 - \phi_1) + l_5\sin(\phi_2 - 3\phi_1) + l_6\sin(\phi_2 + 3\phi_1)] \\
& + \frac{r_2^3}{r_1}[l_7\sin(\phi_1 + 3\phi_2) + l_8\sin(\phi_2 + \phi_1)]\}
\end{aligned} \tag{124}$$

$$
\begin{aligned}
\dot{\phi_2} = & \, Im(A_1) + Im(A) r_2^2 \\
& + \epsilon \{ \frac{r_1}{r_2} [l_1 \sin(\phi_1 - \phi_2) + l_2 \sin(\phi_2 + \phi_1)] \\
& + r_1 r_2 [l_4 \sin(\phi_2 + \phi_1) \\
& + l_3 \sin(\phi_1 - \phi_2) + l_5 \sin(\phi_1 - 3\phi_2) + l_6 \sin(\phi_1 + 3\phi_2)] \\
& + \frac{r_1^3}{r_2} [l_7 \sin(\phi_2 + 3\phi_1) + l_8 \sin(\phi_2 + \phi_1)] \}
\end{aligned} \tag{125}
$$

where δ in the last two equations is the imaginary part of constant A_{21}.

Bibliography

[1] P. Berens. Circstat: A matlab toolbox for circular statistics. *Journal of Statistical Software*, 31, 2009.

[2] DC et al. Bullock. Compact and easy-to-use tungsten-in-glass microelectrode manufacturing workstation. *Medical and Biological Engineering and Computing*, 26:669–672, 1988.

[3] Laurel H. Carney et al. Suboptimal use of neural information in a mammalian auditory system. *The Journal of Neuroscience*, 34:1306–1313, 2014.

[4] S. Coombes, R. Thul, J. Laudanski, A.R. Palmer, and C.J. Sumner. Neuronal spike-train responses in the presence of threshold noise. *Frontiers in Life Science*, 5:3-4:91–105, 2011.

[5] Thomas Duke, Daniel Andor, and Frank Julicher. Physical basis of interference effects in hearing. *Annales Henri Poincaré*, 4:667–669, 2003.

[6] Taffeta M. Elliott and Frédéric E. Theunissen. The modulation transfer function for speech intelligibility. *PLOS Computaitonal Biology*, 5, 2009.

[7] Lea et al. Fredrickson-Hemsing. Mode-locking dynamics of hair cells of the inner ear. *PHYSICAL REVIEW E*, 86, 2012.

[8] Armin Fuchs. *Nonlinear Dynamics in Complex Systems: Theory and Applications for the Life-, Neuro- and Natural Sciences*. Springer, 2013 edition, 2012.

[9] John Guckenheimer and Yuri A. Kuznetsov. Fold-hopf bifurcation. *Scholarpedia*, 2(10):1855, 2007.

[10] A.L. Hodgkin. The local electric changes associated with repetitive action in a non-medullated axon. *Journal of Physiology*, 107:165–181, 1948.

[11] Frank C. Hoppensteadt and Eugen M. Izhikevich. *Weakly Connected Neural Networks*, volume 126 of *Appied Mathematical Sciences*. Springer, 1997.

[12] Eugen M. Izhikevich. *Dynamical Systems in Neuroscience*. The MIT press, 2007.

[13] Eugene M. Izhikevich. Neural excitability, spiking and bursting. *International Journal of Bifurcation and Chaos*, 10, No.6:1171–1266, 2000.

[14] Eugene M. Izhikevich. Simple model of spiking neurons. *IEEE Transactions of Neural Networks*, 14:1569–1572, 2003.

[15] Timothy J. Lewis and John Rinzel. Dynamics of spiking neurons connected by both inhibitory and electrical coupling. *Journal of Computational Neuroscience*, 14:283–309, 2003.

[16] SCHREINER C.E. JORIS, P.X. and A. REES. Neural processing of amplitude-modulated sounds. *Physiol Rev*, 84:541–577, 2004.

[17] Frank Julicher. Mechanical oscillations at the cellular scale. *[physics.bio-ph]*, arXiv:physics/0106071, 2001.

[18] JC Kim and EW Large. Signalprocessing in periodically forcedgradient frequency neural networks. *Front. Comput. Neurosci.*, 9:152, 2015.

[19] Youngtae Kim. Identification of dynamical states in stimulated izhikevich neuron models by using a 0-1 test. *Journal of Korean Physical Society*, 57(6):1363–1368, 2010.

[20] Edward W. Large, Felix V. Almonte, and MArc J. Velasco. A canonical model for gradient frequency neural networks. *Physica D*, 239:905–911, 2010.

[21] Edward W. Large and John D. Crawford. Auditory temporal computation: Interval selectivity based on post-inhibitory rebound. *Journal of Computational Neuroscience*, 13:125–142, 2002.

[22] Edward.W. Large. *Signal Processing, Plasticity and Pattern Formation in Networks of Neural Oscillators.*

[23] EW Large and FV Almonte. Neurodynamics, tonality, and the auditory brainstem response. *Annals of the New York Academy of Sciences*, 1252:E1–E7, 2012.

[24] E.W. Large, J. Kozloski, and J.D. Crawford. A dynamical model of temporal pro- cessing in the fish auditory system. *Proceedings of the Association for Research in Otolaryngology. Abst.*, 21:717, 1998.

[25] Jonathan Laudanski et al. Mode-locked spike trains in responses of ventral cochlear nucleus chopper and onset neurons to periodic stimuli. *Journal of Neurophysiology*, 103:1226–1237, 2009.

[26] Sang Gui Lee and Seunghwan Kim. Bifurcation analysis of mode-locking structure in a hodgkin-huxley neuron under sinusoidal current. *Physical Review E*, 73:041924, 2006.

[27] Karl D. Lerud, Felix V. Almonte, Ji Chul Kim, and Edward W. Large. Mode-locking neurodynamics predict human auditory brainstem responses to musical intervals. *Hearing Research*, 308:41–49, 2014.

[28] J. E. Marsden and M. McCracken. *The Hopf Bifurcation and Its Applications*, volume 19 of *Applied Mathematical Sciences*. Springer-Verlag, 1976.

[29] Alastair McAulay. Modeling neural netwroks with lasers. *SPIE Newsroom*, DOI: 10.1117/2.1200601.0018, 2006.

[30] Myongkeun Oh and Victor Matveev. Loss of phase-locking in non-weakly coupled inhibitory networks of type-i model neurons. *Journal of Computational Neuroscience*, 26:303–320, 2009.

[31] Arkady Pikovsky, Rosenblum Rosenblum, and Jurgen Kurts. *Synchronization, A universal concept in nolinear sciences*. Cambridge nonlinear science series 12. Cambridge University Press, 2001.

[32] M.G. Rosenblum, A.S. Pikovsky, and J. Kurths. Phase synchronization of chaotic oscillators. *Physical Review Letters*, 76:1804, 1996.

[33] D.M. Schwarz, M.S.A Zilany, M. Skevington, N.J. Huang, B.C. Flynn, and L.H. Carney. Semi-supervised spike sorting using pattern matching and a scaled mahalanobis distance metric. *J. Neurosci. Methods.*, 206:120–131, 2012.

[34] James P. Sethna. *Statistical Mechanics: Enthropy, Order Parameters, and Complexity*. Clarendon Press, Oxford, 2011.

[35] P. Tass et al. Detection of n:m phase locking from noisy data: Application to magnetoencephalography. *Physical Review Letters*, 81:3291–3294, 1998.

[36] J. Leo van Hemmen, André Logtin, and Andreas N. Vollmayr. Testing resonating vector strength: Auditory system, electric fish, and noise. *Chaos, An Interdisciplinary Journal of Nonlinear Science*, 21, 047508, 2011.

[37] Stephen Wiggins. *Introduction to Applied Nonlinear Dynamical Systems and Chaos*, volume 2 of *Texts in Applied Mathematics*. Springer, 2 edition, 2003.

[38] Hugh R. Wilson and Jack D. Cowan. Excitatory and inhibitory interactions in localized populations of modeled neurons. *Biophysical Journal*, 12, 1972.

[39] P. Yu. Computation of the simplest normal forms with perturbation parameters based on lie transformation and rescaling. *Journal of computational and applied mathematics*, 144:359–373, 2002.